AALBORG UNIVERSITY ESBJERG

Numerical Modelling of a Suction Reed Valve from a Reciprocating Compressor using Fluid Structure Interaction

Master's Thesis in Process Engineering and Combustion Technology

PECT10-2-F18

07-06/2018

AALBORG UNIVERSITY
STUDENT REPORT

Institute of Energy Technology
Niels Bohrs Vej 8
DK-6700 Esbjerg
www.en.esbjerg.aau.dk

Title:
Numerical Modelling of a Suction Reed Valve from a Reciprocating Compressor using Fluid Structure Interaction

Theme:
Master's Thesis in Process Engineering and Combustion Technology

Project period:
Spring Semester 2018

Project group:
PECT10-2-F18

Members:
Kasper Holst Fornitz

Rasmus Frost Hansen

Supervisor:
Matthias Mandø

Contact person:
Jørgen Houe Pedersen - Nidec, Flensborg

No. of Pages: 72

No. of Appendix Pages: 7

Total no. of pages: 79

Completed: 07-06/18

Abstract:

This project is suggested by Nidec Global Appliance Germany GmbH. The company is interested in using CFD models to boost their development phase of hermetically sealed reciprocating compressors.
In this thesis both a lumped model and a 2-D planar CFD/FSI model is set up in order to determine the dynamic response of a suction valve.
The lumped model is based on non-steady valve flow equations. The lumped model is set up in MATLAB and is compared to data from computer simulation program KV-DYN due to lack of experimental data.
The 2-D planar CFD/FSI model of a compressor is set up in ANSYS Fluent. The dynamic mesh method is used to account for the movement of the piston and the valve displacement. The CFD/FSI model is also compared to the data from KV-DYN.
The CFD/FSI model and the lumped is not directly compared given the lumped model is simplified to such an extended a comparison is difficult. The lumped is able to capture some features of a compressor cycle, among them, to a lesser extent the dynamic response of the suction valve.
The CFD/FSI model is able to describe the non-steady flow phenomena in valve channels and the compressor cycle.
It is expected the models can be used in the design phase of compressors if they are improved.

## Acknowledgement

We would like to thank Jørgen H. Pedersen from Nidec's department in Flensborg for being at our disposal, in person as well as through mail correspondence, the entire project period. Jørgen's knowledge and passion for designing and optimising compressors has been inspiring and helped us throughout the entire project period. Jørgen has been a great sparring partner, listening to our ideas and discuss them with us.

Contents

1. Introduction **1**
1.1. Background 4
1.2. Reading Guide 7

2. Mass-Spring-Damper System **8**
2.1. Free Oscillations 8
2.1.1. Undamped System 9
2.1.2. Damped System 10

3. Lumped Model **13**
3.1. Description of Non-Steady Gas Flow in the Suction Valve Channel 14
3.2. Non-Steady Valve Flow Equations 15
3.2.1. Valve Motion Equation 17
3.2.2. Gas Flow 18
3.2.3. Pressure Difference 20
3.2.4. Cylinder Volume 20
3.3. KV-DYN 21
3.4. Assumptions for the Lumped Model 22
3.5. Implementation to MATLAB 23
3.5.1. Code Setup Approach 24

4. CFD/FSI Model **27**
4.1. Geometry 27
4.2. Dynamic Mesh 29
4.2.1. Transport Equations 29
4.2.2. Remeshing 30
4.2.3. Smoothing 31
4.2.4. Layering 32
4.3. Troubles with Axisymmetry Geometry 33
4.4. User Defined Function 35
4.4.1. Macros 35
4.5. Degrees of Freedom 36
4.6. Event Mode 37
4.7. Discretization Method 37
4.8. Grid Independency Analysis 38
4.9. Turbulence Model 40
4.9.1. Energy Equation 41
4.10. Assumptions 42

5. Results and Discussion **43**
5.1. KV-DYN Results 45

5.2. CFD/FSI Results 47
5.2.1. Imagery Illustration of a Piston Revolution 47
5.2.2. Comparison of the CFD/FSI Model and KV-DYN 52
5.2.3. Discussion of Results 53
5.3. Lumped Model Results 54
5.3.1. Comparison of Code and KV-DYN 56
5.3.2. Discussion of Results 56

6. Conclusion **59**

Appendix **62**
A. Code used to Generate the Lumped Model Results 62
B. Results from code without clearance volume 66

Abbreviations, Symbols and Nomenclature

Table 1: Abbreviations

Abbreviations	Full meaning
2-D	Two Dimensional
3-D	Three Dimensional
App.	Appendix
BDC	Bottom Dead Center
CFD	Computational Fluid Dynamics
Eq.	Equation
Fig.	Figure
FSI	Fluid Structure Interaction
ODE	Ordinary Differential Equation
SDD	Simulation Driven Design
SDOF	Single Degree-of-Freedom
Tab.	Table
TDC	Top Dead Center
UDF	User Defined Function

Table 2: Symbol list

Symbol	Definition	SI unit
a	Acceleration	$\frac{m}{s^2}$
a	Crank radius	m
A	Area	m^2
A_p	Port area	m^2
A_L	Opening area	m^2
A_2	Effective flow area	m^2
$A(s)$	Varying cross section along a streamline	m^2
A_j	jth face area	m^2
B	Diameter of the cylinder	m
c	Damping coefficient	Ns/m
c_p	Force coefficient	-
c_p	Specific heat	$\frac{kJ}{kgK}$
C_1, C_2	Arbitrary coefficients	-
C_D	Discharge coefficient	-
d	Diameter of the port area	m
D	Diameter of the valve	m
E_{kin}	Kinetic energy	J
f	Natural frequency	$\frac{1}{s}$
F	Sum of all forces acting on the valve	N
F_0	Any other force (sticktion, pre-tension)	N
F_1	Spring force	N
F_2	Damping force	N
F_g	Gravitational force	N
F_{pl}	Flow induced force on valve plate	N
G_k	Generation of turbulent kinetic energy	$\frac{J}{kg}$
h	Time step size	s
h_{min}	Minimum cell height of the layer adjacent to the boundary	m
h_{ideal}	Ideal cell height	m
J	Gas inertia parameter	-
k	Spring stiffness	$\frac{N}{m}$
k	Turbulent kinetic energy	$\frac{J}{kg}$
k (Energy Eq.)	Thermal conductivity	$\frac{W}{mK}$
l	Length of spring at rest	m

L	Length of seat edge	m
L_{rod}	Connection rod length	m
m	Mass of refrigerant	kg
M	Mass of valve	kg
M^*	Mass of spring	kg
M_{molar}	Molar weight of refrigerant	$\frac{g}{mol}$
n	Number of iterations	-
n_f	Number of faces on the control volume	-
P	Pressure	Pa
r	Cylinder volume correction coefficient	-
R	Gas constant	$\frac{kJ}{kmolK}$
RPM	Compressor speed	$\frac{1}{min}$
s	Mean streamline through a valve channel	-
S_Φ	Source term of general scalar	-
T	Temperature	K
u	Velocity	$\frac{m}{s}$
u_g	Velocity of the moving mesh	$\frac{m}{s}$
v_{spring}	Velocity of the spring	$\frac{m}{s}$
V	Volume	m^3
V_G	Translation motion	-
W_2	Velocity of emerging gas jet	$\frac{m}{s}$
Y	Valve displacement/lift	m
Y_M	Effect of compressibility	$\frac{kg}{ms^3}$
æ	End correction coefficient	-
Greek Symbols:		
α	Thermal conductivity	$\frac{W}{mK}$
α_k, α_ϵ	Inverse effective Prandtl number	-
α_s	Layer split factor	-
Γ	Diffusion coefficient	$\frac{m^2}{s}$
δ	Kronecker delta	-
Δ	Difference	-
ϵ	Turbulent dissipation rate	$\frac{J}{kgs}$
θ	Crank angle	$^\circ$, rad
μ	Viscosity	Pas
λ	Solutions to characteristic equation	-
ξ	Displaced distance of intermediate point	m

ρ	Density of refrigerant	$\frac{kg}{m^3}$
τ	Stresses	$\frac{N}{m^2}$
ϕ	General scalar	-
ω	Angular velocity	$\frac{rad}{s}$
ω_0	Angular natural frequency	$\frac{rad}{s}$
ω^*	Damped natural frequency	$\frac{rad}{s}$

Indices and super-/subscripts		
$\dot{}$	Derivative with respect to time	
$\ddot{}$	Double derivative with respect to time	
$\vec{}$	Vector	
$\bar{}$	Mean/average	
$'$	Fluctuating	
cyl	Cylinder	
dis	Discharge	
eff	Effective	
i	Component in the i-direction	
j	Component in the j-direction	
k	Component in the k-direction	
suc	Suction	
t	Turbulent	

1. Introduction

This project is suggested by Nidec Global Appliance Germany GmbH. This department of Nidec is highly specialized in designing hermetically sealed reciprocating compressors. This department's mission is to make refrigeration and cooling systems more effective, more efficient, and more responsible given compressors are an important topic since they are needed in many applications in the modern day industries and homes. For the ever increasing demand of compressors and their reliability together with economic demands, the development of compressors have to be addressed. The development phase of compressors can be boosted by creating reliable Computation Fluid Dynamics (CFD) models. This is the agenda for Nidec and therefore the main topic of this thesis.
The first approach for determining the dynamic response of reed valves in a hermetically sealed reciprocating compressor is based on simple mathematical models. Integral formulations are used to evaluate the compression process inside the cylinder and semi-empirical expressions are used to determine the mass flow of refrigerant through the valve channels as well as the dynamics of the valves [1]. This type of model is called a lumped model. Given lumped models are based on semi-empirical expression, there are parameters in the expressions set by the user. These are e.g. parameters such as the discharge valve coefficient, an entrance loss coefficient, and the valve plate force coefficient. Lumped models are reliable and are able to determine the dynamic response of reed valves within a few seconds of calculation time. However, the reliability of lumped models depend on the user's inputs. The user has to have experience with designing compressors in order to input valid values into the lumped model. Lumped models are used as an initial approach in the development phase of compressors. Inappropriate design of compressors can lead to the valves oscillate to much, meaning it will hit the piston. This increases the noise level and the wear on the compressor. In worst case the valve can break.
In order to boost the development phase, Simulation Driven Development (SDD) is beneficial. SDD is used to design Two-Dimensional (2-D) or even Three-Dimensional (3-D) CFD models. The use of CFD models are advantageous in several ways. CFD models does not require any assumptions as the lumped models do and input parameters based on the designers experience is not required. Therefore CFD models can be used to validate these assumptions in an early state of the compressor development phase. Furthermore, flow features are included in the CFD models. The design of the compressor can easily be changed and optimised with the information gained from CFD models. In addition, when using CFD models acoustics can be taken into account. So far acoustics are investigated by performing experiments. Experiments are difficult to perform given a proper setup is required, but especially because the compressor is sealed. There are also some disadvantages when using CFD models. The design process of CFD models as well as the computational cost is significantly larger compared to lumped models. If CFD models are designed properly they are more reliable than lumped models and can reflect the actual dynamics of reed valves to a great extent. There is also an economic perspective to take into account. Instead of producing different prototypes, SDD is used to design the optimal design for the compressor and afterwards the prototype is pro-

duced. This process decreases the material costs and for this reason the development of applicable CFD models are of great interest.

The dynamics of the reed valve depends strongly on the piston movement and the design of the mufflers. The response is also strongly dependent on the damper in the system. In compressors the damping effect is dependent of the refrigerant flow across the reed valve. Mufflers are not taken into account in this study since acoustics is not modelled. The task for hermetically sealed reciprocating compressors are to increase the pressure of the gas in the cylinder. A simplified illustration of a reciprocating compressor is given in Fig. 1.

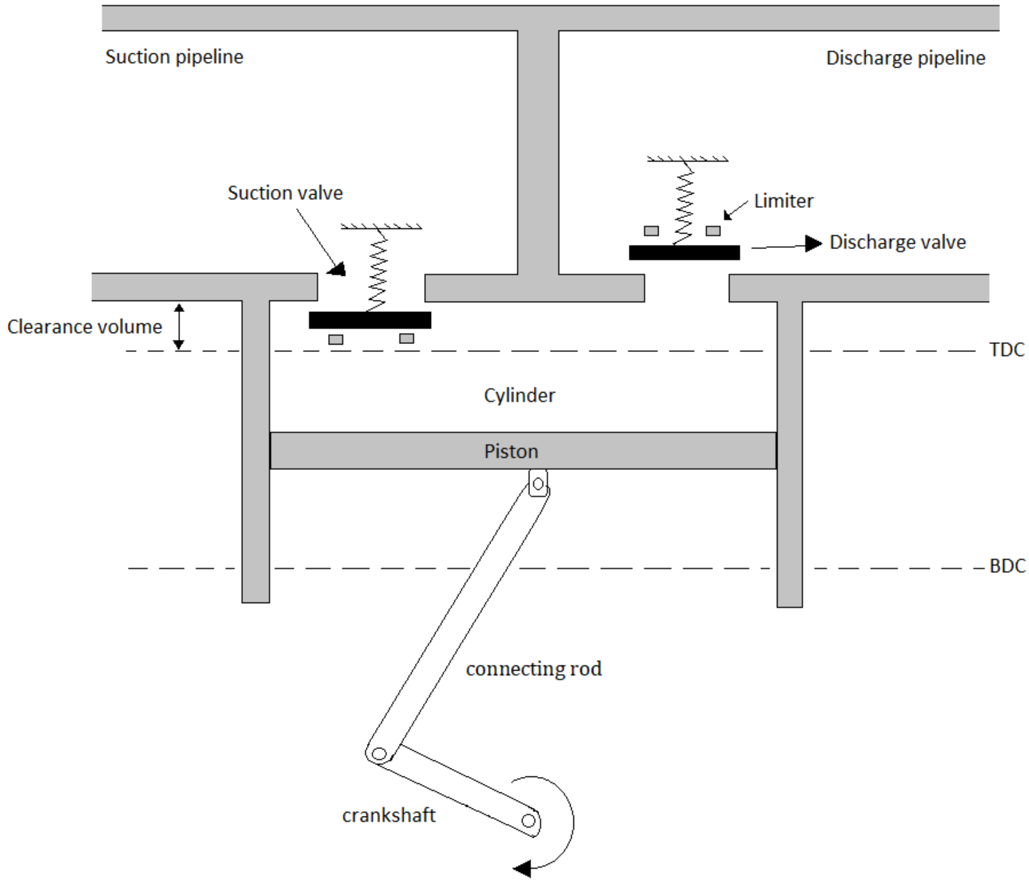

Figure 1: Simplified illustration of a reciprocating compressor. Modified from [2]

A reciprocating compressor consist of a cylinder, a piston, a crankshaft, a connection rod, and suction and discharge valves. These are the main parts of a compressor. When the piston is at Top Dead Center (TDC), the volume of the cylinder is only the clearance volume. When the piston is at Bottom Dead Center, the cylinder is at its maximum volume. The compressor is connected to suction- and discharge pipelines. Fig. 2 illustrates a typical reed valve used in reciprocating refrigeration compressors.

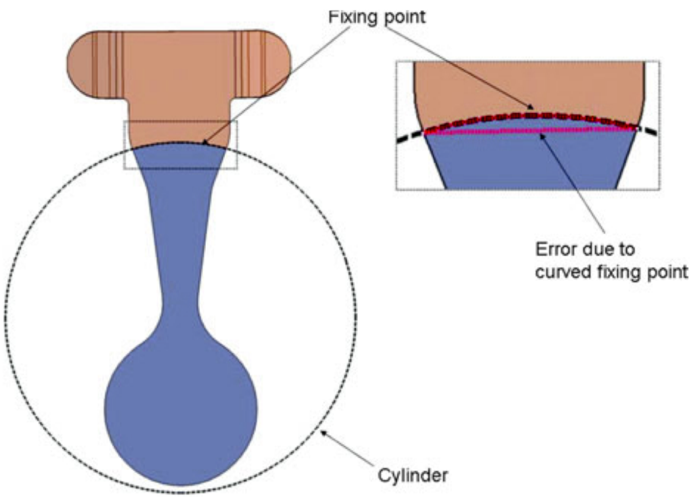

Figure 2: Illustration of a reed valve [3]

The ideal compressor cycle is illustrated in Fig. 3. A detailed description of the cycle illustrated in Fig. 3 is based on the references [4, 5].

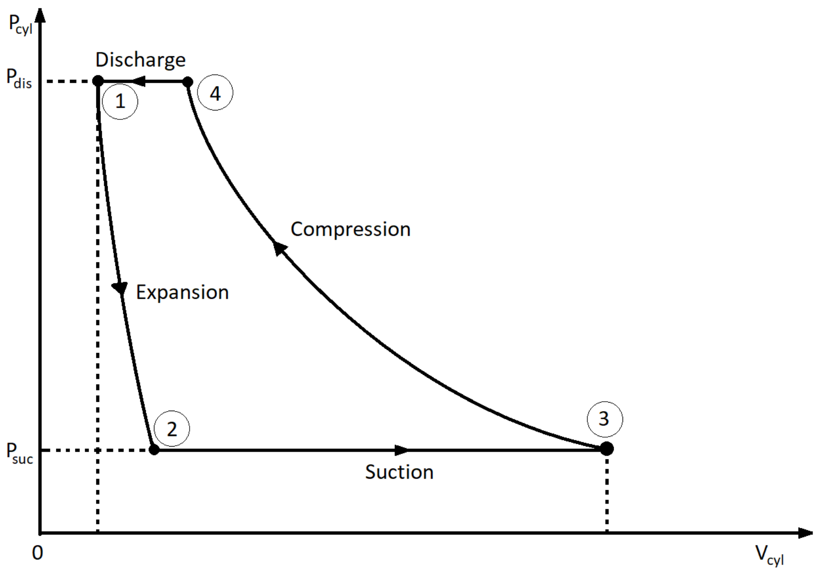

Figure 3: P-V diagram of an ideal compressor cycle. Modified from [6]

Fig. 3 illustrates a cylinder P-V diagram for an ideal compressor cycle. In the figure, P_{cyl}, P_{dis}, and P_{suc} is the cylinder, discharge, and suction pressure, respectively. V_{cyl} is the volume of the cylinder. The area in the cycle is proportional with the work transferred from the moving piston to the gas, per cycle [7].
At position 1 the cylinder is at TDC. Here both the suction and discharge valves are closed. Then the piston starts to move toward BDC and shortly after the suction valve opens. This is position 2 in the figure. The suction valve opens since the pressure in the cylinder is lower than the pressure in the suction pipeline. The volume of the cylinder is increased until the piston reach BDC. This is position 3. When the piston has reached BDC and the cylinder is filled with refrigerant the piston start moving towards TDC again. The refrigerant is compressed and the pressure increase. As compression of the gas starts, the suction valve is once again closed given the pressure in the cylinder is higher than the pressure in the suction pipeline. The compression of gas continues until the discharge valve opens. This is position 4. The discharge valve opens when the pressure in the cylinder is higher than the pressure in the discharge pipeline and the compressed refrigerant flows into the discharge pipeline. Some of the compressed gas will remain in the clearance volume. This expansion and compression process is repeated.

As mentioned in the beginning of the introduction it is attractive to use CFD models in the development phase of hermetically sealed reciprocating compressors given these models provide more information compared to lumped models. CFD models do not need values for certain flow input parameters. The objective of this study is to determine the dynamics of a suction valve and to investigate if a CFD model can boost the development phase of this type of compressor. Two models are set up, a lumped model in MATLAB and a 2-D CFD model combined with Fluid Structure Interaction (FSI) in ANSYS Fluent. The work approach in this thesis is parallel, meaning each author is mainly focused on setting up one model each. This intend is to have two comparable models as a final result. These two models have identical geometric input parameters and is compared with respect to the dynamic response. In order to validate the reliability of these two models, they are compared to data from the computer simulation program KV-DYN. KV-DYN calculates the dynamic processes of both suction and discharge reed valves. The data is provided by a contact person from Nidec Global Appliance Germany GmbH in Flensborg. The data is provided by the company in the lack of experimental measurement.

1.1. Background

A study by L. Böswirth [8, 9] discussed the possibilities of setting up a model where non-steady flow effects through valve channels are taken into account. Böswirth found gas inertia effects are of great importance. In order to set up the model, Böswirth made adequate simplifications so the complexity of the problem was reduced, and a manageable system of equations was obtained. First Böswirth investigated the steady state flow concept. Then basic equations accounting for gas inertia effects were investigated. Böswirth set up an example in order to investigate the effect of inertia when the lift

height of the valve was fixed and a constant pressure difference across the valve was applied for a given time interval. Böswirth found that this problem had an analytic solution. In another example a constant mean pressure difference across the valve was assumed by applying a sinusoidal pressure distribution. In order to solve this problem Böswirth found an adequate approximation solution, since the problem otherwise not could be solved analytically. Then Böswirth investigated full non-steady flow equations where the fixed lift height of the valve was dropped. Once again adequate simplification were required in order to solve the problem analytically. Böswirth assumed sinusoidal velocity variations caused by the forced sinusoidal movement of the valve, and the pressure difference across the valve to be constant.
Following Böswirth investigated the flow force on the valve plate. The momentum theorem and a control volume was used to derive an expression for the flow force under non-steady flow conditions. Böswirth found that there was no reason to introduce a frictional force because inertia effect already had been taken into account in the flow process. In order to investigate the effect of gas inertia, Böswirth tested the new derived equations for several different cases with the purpose of finding solutions for each case. Böswirth also investigated how the inertia parameters are influenced by the valve dimensions. Böswirth concluded the gas inertia effect is accessible to mathematical computations.
Böswirth carried out non-steady flow experiments with enlarged models [10] to back the theoretical insights in [8, 9]. Since the complexity of the problem is very high, the simplest case was studied. The valve plate is at a fixed position and non-steady flow effects are due to rapid changes in the pressure difference across the valve only. Böswirth found this sharp pressure pulse first accelerates the gas in the valve channel, and following charge the valve, meaning that the pressure pulse acts with a time delay, and therefore with a reduced force amplitude on the valve. Böswirth concluded the non-steady flow model for valve flow in [8, 9] was confirmed by the valve flow experiments.
Later on Böswirth published another study [11, 12]. In this study valve flutter was investigated theoretically and experimentally. Using classical theory of stability and the assumption of constant inflow and outflow to the system, Böswirth was able to predict the onset of valve flutter. Böswirth proposed valve flutter is controlled by six dimensional constants only: a mass transfer parameter, a gas spring parameter, a spring characteristic parameter, a damping parameter, a gas inertia parameter, and a non-steady flow parameter. Flutter experiments with an enlarged model was carried out to test the reliability of these six parameters. The theoretical model was in agreement with the experimental results. Based on this, Böswirth found the basic equations presented in [8, 9, 10] could be improved if valve flutter was taken into account. These improvements make the model more precise.
Böswirth round off the work about non-steady flow in valves presented in [8, 9, 10] with another study [13]. In this study Böswirth presents a manageable system of equations describing the non-steady flow in valve channels. This system of equations accounts for gas inertia effects and non-steady work between the gas flow and the valve. In order to account for valve flutter phenomena a gas-spring-effect was found to be essential. Böswirth found the damping force on a valve depend on the squeezed gas flow between

the valve seat and the valve. Based on the detailed work, Böswirth presented a valve dynamic simulation program, named KV-DYN, able to calculate the important dynamic processes in suction and discharge valves of hermetic refrigeration compressors [14].

In the study by Matos et al. [15] a 2-D computational model was developed to simulate the dynamic process of reed valves of reciprocating compressors. In order to account for the valve motion, a Single Degree-Of-Freedom (SDOF) model was used. Using a moving coordinate system it was possible to account for the valve displacement, whether the spring was expanded or compressed. The flow field through the valve channel was assumed turbulent, axisymmetric, and incompressible. The flow field was solved by the finite volume methodology. The results from the study include information about the turbulent flow through the valve channel and the valve motion.
The piston motion is not described in this study, but on the other hand a periodic flow rate through the valve channel is prescribed at the valve channel entry. The RNG $k-\epsilon$ model was used to solve the turbulent flow through the valve channel.
As an initial case the study tested two scenarios: fixed valve lift and harmonically valve lift. These scenarios were compared with experimental data and were in good agreement. Therefore, the methodology was used for further tests.
The study concluded a sinusoidal flow rate condition at the valve channel entrance, was able to resolve some of the features of the valve dynamics. Furthermore, the study concluded compressibility effect of the gas should be included. Also, the mass flow rate through the valve channel should not be a prescribed value, but a function of the pressure difference across the valve.
One of the co-authors continued work on the methodology. This study by Pereira et al. [1] developed three simulation models for a reciprocating refrigeration compressor. A 1-D, a 2-D, and a 3-D simulation model. For each model a SDOF model was chosen and the governing flow equations were discretized using a finite volume methodology. The results of the study include among others the valve displacement of the suction and discharge valve.
The 1-D model is solved for mass, momentum and energy balance for a compressible fluid. The reed valve is influenced by the flow induced force acting on it. This force, as well as the mass flow rate through the valve channel is dependent on the effective flow area and effective force area.
The turbulent flow in the valve channels and in the cylinder in the 2-D and 3-D model were modelled using the RNG $k-\epsilon$ model. In order to simulate the compression process for the cylinder and the movement of the valve, a moving grid strategy was applied. For the 2-D model an axisymmetric domain was chosen.
The study found the 3-D model, with respect to the suction process, was in very good agreement with the experimental data, but there were observed some discrepancies for the discharge process. The study found the 2-D and 3-D model were in good agreement, but the 1-D model did show some quite different results. The damping coefficient affected the 1-D model much more than the 2-D and 3-D model. The study concluded the computationally cheaper models (1-D and 2-D) are applicable as a first try when designing a compressor.

1.2. Reading Guide

The two models created in this thesis are modelled as a SDOF mass-spring-damper system. In Sec.2 the general mass-spring-damper system with free oscillations is introduced. In Sec.3 the lumped model is presented. The lumped model is a mass-spring-damper system with external forced oscillations. The basic equations used when setting up the lumped model are presented in this section, as well is the assumptions used when setting up the model. KV-DYN is also introduced in this section, given the lumped model is based on the same basic equations as KV-DYN. The implementation of the equations in MATLAB is also described in this section. After the lumped model is introduced, the second part of this thesis is introduced, namely the CFD/FSI model. In Sec.4 all the methods used to set up the 2-D CFD/FSI is introduced and described. The creation of User Defined Functions (UDF), the use of Fluent's 6DOF solver, how to implement a dynamic mesh in order to account for the movement of the piston and valve, and the use of an event-mode to create a temporary outlet is covered. This section also include information of how the refrigerant is treated and what turbulence model is used. A grid independency analysis is included in this section. In Sec.5 the results from the lumped model, the 2-D CFD/FSI model, and KV-DYN is compared. Differences and similarities between the models and the reliability of each individual model is discussed in this section as well. Finally the conclusion summarises the findings in this thesis.

2. Mass-Spring-Damper System

In this section a SDOF system, in the form of a mass-spring-damper system is investigated. A SDOF system means the valve only can move in one direction. The motion of the mass-spring-damper system is investigated for free oscillations. This section is based on the describtion found in the textbook "Advanced Engineering Mathematics" by Erwin Kreyszig. [16]

2.1. Free Oscillations

Fig.4 illustrate the model investigated.

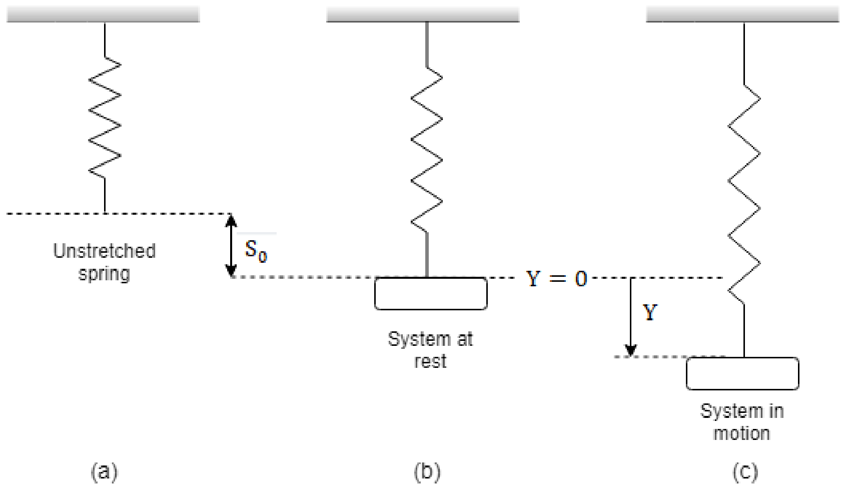

Figure 4: Mass-spring system [16]

The model consist of a spring, which can be extended as well as compressed. The spring is attached to a fixed support. At the end of the spring the valve is attached. When the system is at rest, the position of the valve is given by $Y = 0$. The downward direction is chosen as positive, thus the gravitational force acting on the valve is positive. When the system is in motion, the valve is moved by a distance, $Y > 0$. This is illustrated in Fig. 4c. This motion causes a spring force proportional to the extended distance of the spring, Y, with the spring constant k. k is the spring stiffness. This is Hooke's law and is expressed by Eq.(1).

$$F_1 = -kY \tag{1}$$

The spring force, F_1, is directed against the displacement, thus the minus sign. The spring force is also known as a restoring force, given it want to restore the system back to its original position at $Y = 0$.
Using Newton's second law, the motion of the mass-spring system in Fig.4 is determined. The expression is given by Eq.(2).

$$Ma = M\ddot{Y} = F \tag{2}$$

Where M is the mass of the valve, a is the acceleration, $\ddot{Y}$ is the second derivative of the position Y, and F is the sum of all forces acting on the valve. $M\ddot{Y}$ is inertia forces.

2.1.1. Undamped System

Now the motion of the mass-spring system is established, an ordinary differential equation (ODE) is set up for an undamped system. An undamped system is a system that would keep oscillate forever. This is illustrated in Fig.5.

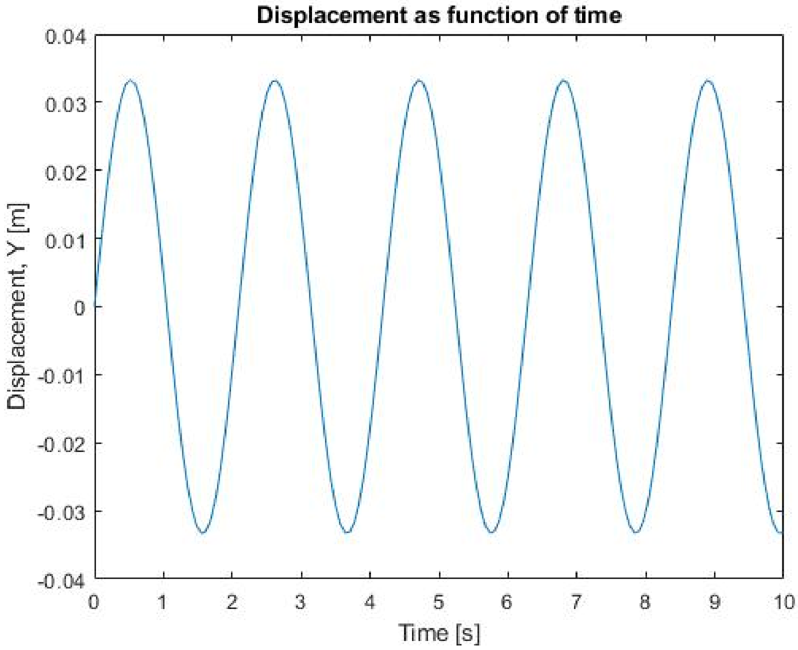

Figure 5: Undamped system

However, every real system is damped. The damping effect can be neglected if the motion of the system is over a short time and the damping is small. From Newton's law, $F = -F_1$ gives $M\ddot{Y} = -F_1 = -kY$. Thus the ODE for an undamped system is given by Eq.(3).

$$M\ddot{Y} + kY = 0 \tag{3}$$

As mentioned before, $Y = 0$ defines the equilibrium position of the valve. Eq.(3) is a second order homogeneous linear ODE with constant coefficients. The general solution to Eq.(3) is given by Eq.(4).

$$Y(t) = Acos\,(\omega_0 t) + Bsin\,(\omega_0 t) \tag{4}$$

Where A is the value of Y at time $t = 0$. The value of B is the initial velocity of the system, $\dot{Y}(0)$, which is equal to $\omega_0 B$. ω_0 is the angular natural frequency, defined by:

$$\omega_0 = \sqrt{\frac{k}{M}}$$

Eq.(4) describes a harmonic oscillation motion with frequency $f = \omega_0/2\pi$. f is the natural frequency of the system [17].

2.1.2. Damped System

As mentioned previously, every real system is damped. A damping force is added to the model, Eq.(3). The expression for the damping force can be expressed as Eq.(5) and Fig.6 illustrates a system where a damper is included.

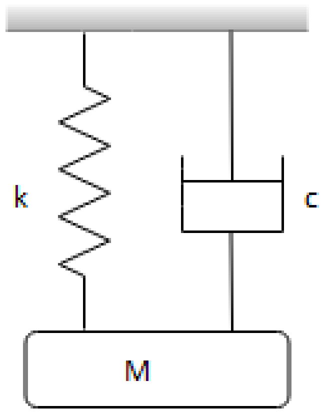

Figure 6: Mass-spring-damper system

$$F_2 = -c\dot{Y} \tag{5}$$

Where c is the damping coefficient (always a positive value) and $\dot{Y}$ is the velocity of the valve. The damping force is proportional to the velocity. Eq.(6) is an expression for viscous damping.
The ODE for the mass-spring-damper system is then given by Eq.(6).

$$M\ddot{Y} + c\dot{Y} + kY = 0 \tag{6}$$

Eq.(6) is a second order homogeneous linear ODE with constant coefficients. The approach of how to solve this expression is not given in this thesis, but can be found in [16]. Using the approach in [16] the characteristic equation is obtained. The expression is given by Eq.(7).

$$\lambda^2 + \frac{c}{M}\lambda + \frac{k}{M} = 0 \tag{7}$$

Where λ are the solutions to the characteristic equation. These are given by Eq.(8)

$$\lambda_1 = \alpha + \beta \quad \text{and} \quad \lambda_2 = -\alpha - \beta \tag{8}$$

where

$$\alpha = \frac{c}{2M} \quad \text{and} \quad \beta = \frac{1}{2M}\sqrt{c^2 - 4Mk}.$$

The motion of the system depends on the amount of damping, whether there is little damping, medium amount of damping or lot of damping. These three cases are briefly investigated.
In case of underdamping the following criterion is valid:

$$c^2 < 4Mk$$

In this case there are complex conjugate roots, meaning β is imaginary. β is then expressed as follows:

$$\beta = i\omega^* \quad \text{where} \quad \omega^* = \sqrt{\frac{k}{M} - \frac{c^2}{4M^2}}$$

ω^* is the damped natural frequency.
The roots of the characteristic equation is then given by:

$$\lambda_1 = -\alpha + i\omega^* \quad \text{and} \quad \lambda_2 = -\alpha - i\omega^*$$

which has the general solution given by Eq.(9).

$$Y(t) = e^{-\alpha t}\left(Acos\left(\omega^* t + Bsin\left(\omega^* t\right)\right.\right. (9)$$

In the case of critical damping the following criterion is valid:

$$c^2 = 4Mk$$

In this case there is a real double root. Critical damping is a state between oscillation and non-oscillatory motions. The general solution to this case is given by Eq.10.

$$Y(t) = \left(c_1 + c_2 t\right) e^{-\alpha t} \tag{10}$$

Finally, in case of overdamping the following criterion is valid:

$$c^2 > 4Mk$$

In this case there are distinct real roots, λ_1 and λ_2. The general solution for this case is given by Eq.(11).

$$Y(t) = c_1 e^{-(\alpha-\beta)t} + c_2 e^{-(\alpha+\beta)t} \tag{11}$$

Here c_1 and c_2 are arbitrary constants.
Fig. 7 illustrates the difference between an underdamped, a critically damped, and an overdamped system

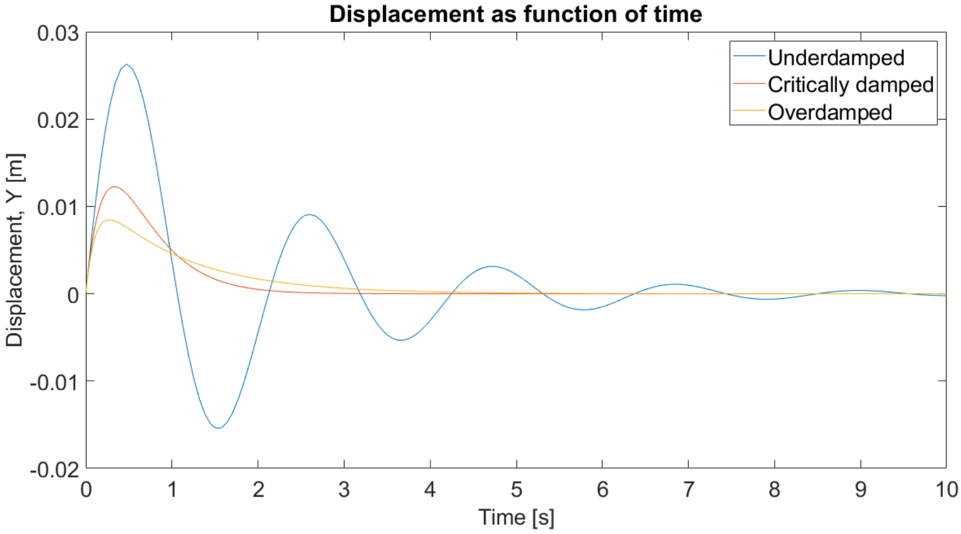

Figure 7: Motion of an underdamped (blue), a critically damped (red), and an overdamped (yellow) mass-spring-damper system

Origin is used as an initial position and 0.1 $\frac{m}{s}$ is used as initial velocity when creating the three different systems.
The blue graph illustrates the motion of an underdamped mass-spring-damper system. The system oscillate about zero until the motion settles at zero on the vertical. The overdamped - and critically damped system also settles at zero on the y-axis. When the system is overdamped (yellow graph), the valve does not oscillate given the energy of the system is taken out quickly by the damper. The critically damped system (red graph) is similar to the overdamper system. Tt appears in the figure, the critically damped system has a larger displacement but is able to settle faster than the overdamped system.

In this section the second order homogeneous linear ODE for a mass-spring-damper system has been investigated when the right hand side of Eq.(6) is zero. In Sec.3 the equation is investigated when the right hand side is non zero and dependent on the flow induced force on the valve plate.

3. Lumped Model

As mentioned in Sec. 1, one part of this thesis is dealing with programming of a lumped model describing valve dynamics of a suction valve in a hermetic sealed reciprocating compressor. This section focuses on presenting the equations needed for setting up a lumped model for non-steady flow. The equations which is used in the lumped model originate primarily from work done by Leopold Böswirth [8, 9, 10, 11, 13, 14].
Differences between KV-DYN and the code created by the authors is discussed and explained in Sec. 5.3.
Fig. 8 illustrates a simplified system of a compressor.

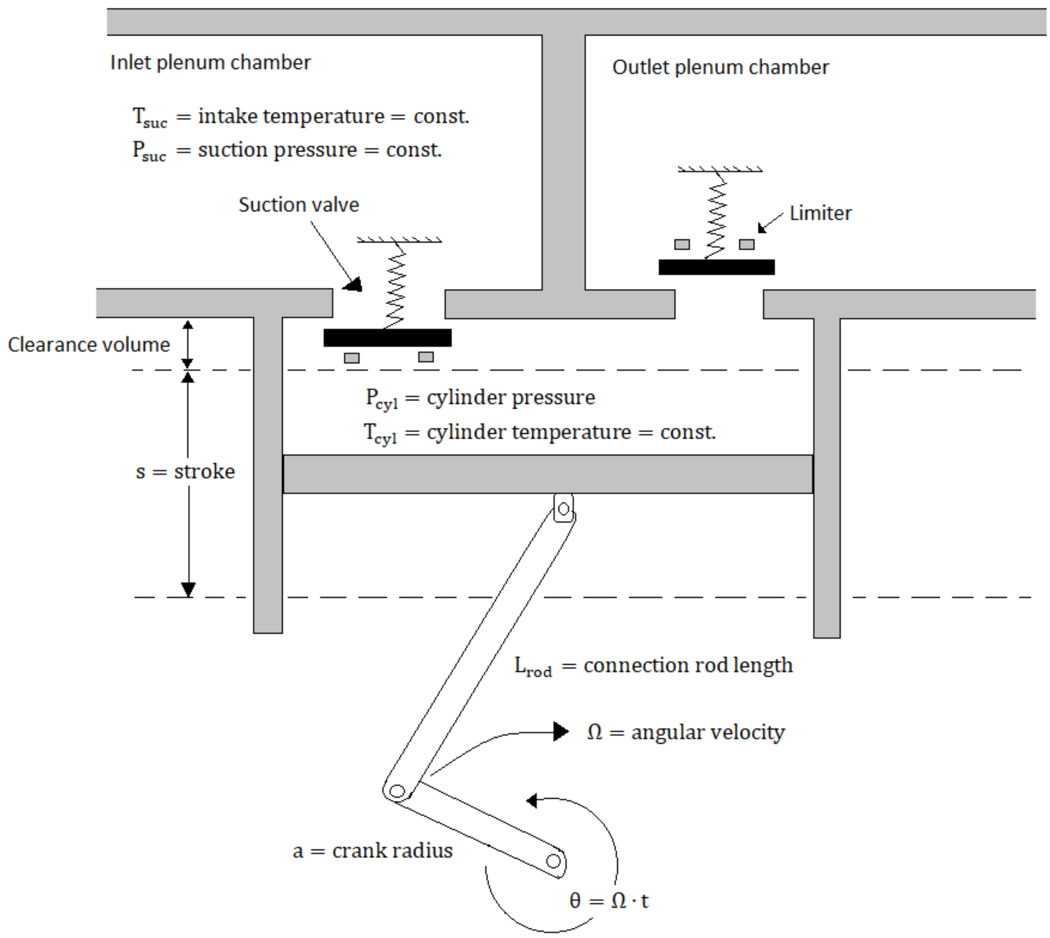

Figure 8: Illustration of the inlet plenum chamber, the cylinder, and the outlet plenum chamber. Modified from [2]

The inlet plenum chamber, the cylinder, and the outlet plenum chamber is given in the figure.

Even though only the suction valve is of interest in this thesis the discharge valve is also illustrated in the figure in order to give an overall impression of the system. The system of interest consist of the inlet plenum chamber and the cylinder. The following assumptions is made to simplify the code. The intake temperature and the suction pressure is constant, as well is the temperature inside the cylinder. The background for these assumptions is explained at a later point in this section.

3.1. Description of Non-Steady Gas Flow in the Suction Valve Channel

This section is based on the description given by Böswirth in [8]. The following description of non-steady gas flow is also valid for the discharge valve channel. The non-steady gas flow can be divided into five phases: three phases accounting for the opening of the valve and two for the closing period. Fig.9 illustrates four of the five phases.

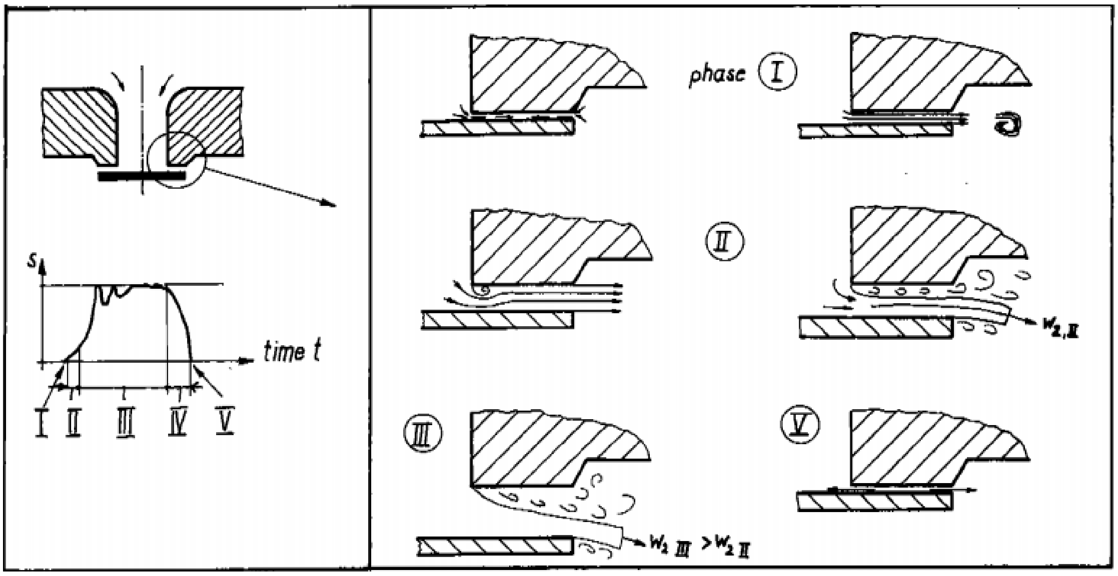

Figure 9: Illustration of four different phases in valve channel flow [8]

In the figure s is the valve lifting height and W_2 is the velocity of the emerging jet.
In the first phase, when the suction valve begins to open, gas flows into the gap and fills it up. When the gap between the valve and the valve seat has been filled with gas, which occurs very fast, the build up of a unidirectional flow field takes place. There is no flow separation at the valve edges, given the gas only has lost an insignificant amount of energy in the newly formed boundary layer. When the first phase is about to end, separation occurs at the seat edge and here the creation of a wake takes place. See Fig. 9.
In the second phase the gab between the seat and valve has become larger. The boundary layers in this phase passes the seat edges. Due to friction the seat edges have lost a great amount of their kinetic energy, which causes separation and wakes to be formed since

the boundary layers are not able to follow the sharp edges of the seat. This phenomena is illustrated in Fig.9. The second phase covers start of separation to full formation of wakes. The duration of this phase is of same order of magnitude as the first phase.
In the third phase the gap between the valve and the seat is as large as possible. In this phase it seems the velocity of the gas has reached steady state, but this is not the case. The gas velocity has still not reached steady state flow. The flow accelerates as it approaches its steady state flow value asymptotically. As it appears in Fig. 9 the velocity of the emerging gas jet is greater in this phase than in the second phase.
As the fourth phase starts, the valve moves against the valve seat. In this phase the flow is decelerated and gas inertia effect is once again created. The gas inertia effect is discussed in Sec. 3.2.2. The deceleration of gas flow takes place even at constant pressure difference across the valve. The same flow pattern as in the third phase (separation and wake formation) is maintained in this phase (see third phase in Fig. 9).
In the fifth and final phase, a gas squeezing effect takes place as the valve plate approaches the seat. As it can be seen in Fig. 9 the gas is squeezed in both directions. [8]
The gas flow through the valve channel is started by the piston movement in the cylinder. When the piston moves, the volume in the cylinder is changed and a pressure difference between the inlet plenum chamber and the cylinder is obtained. When the pressure in the cylinder becomes lower than the pressure in the inlet chamber (suction pressure, see Fig. 8) the force exerted on the valve is able to open the suction valve. When the suction valve opens, gas flows into the cylinder, as well as interact with the valve as it passes through. [18]
Using three basic equations provided by Böswirth along with the motion equation for the mass-spring-damper system the dynamic response of the suction valve can be determined.

3.2. Non-Steady Valve Flow Equations

Eq. (12) is the same as Eq. (6) given in Sec. 2, both describing the motion of the valve. However, this time the right hand of the equation is different from zero. Eq. (13) accounts for the flow induced force on the suction valve, Eq.(14) describes the gas flow through the valve channel, and Eq. (15) is the volume flow rate.

$$M\ddot{Y} + c\dot{Y} + kY = F_{pl} + F_0 \tag{12}$$

$$F_{pl} = A_p \frac{1}{2}\rho W_2^2(t) \tag{13}$$

$$\frac{\Delta P(t)}{\rho} = \frac{W_2^2(t)}{2} + J\left[\dot{W}_2(t)Y(t) + W_2\dot{Y}(t)\right] + \frac{c_p A_p W_2(t)\dot{Y}(t)}{2LC_D Y(t)} \tag{14}$$

$$\dot{V}(t) = LC_D W_2(t) Y(t) \tag{15}$$

Here M is the mass of the valve, c is the damping coefficient, k is the spring stiffness, and F_{pl} is the flow force acting on the valve plate. F_0 takes any other force into account, this could e.g. be a sticktion force nor a pre-tension force on the valve [1]. $\ddot{Y}$, $\dot{Y}$, and Y

is the acceleration, velocity and displacement of the suction valve, respectively. ΔP is the pressure difference across the valve, ρ is the density of the gas, W_2 is the velocity of the emerging gas jet, J is a gas inertia parameter, c_p is a force coefficient, A_p is the port area, L is the length of the seat edge, $\dot{V}$ is the volume flow rate, and C_D is a discharge coefficient.
Geometry and lift height dependent parameters are given in Fig. 10.

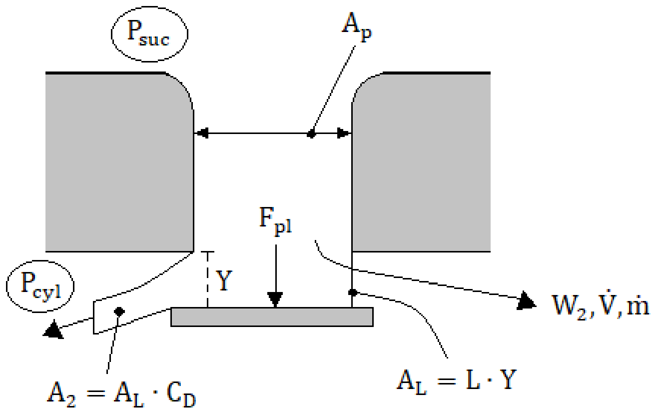

Figure 10: Illustrates geometry and lift height dependent parameters. Modified from [8, 13]

In the figure, A_L is the opening area, A_2 is the effective flow area, and $\dot{m}$ is the mass flow rate. The effective flow area is identical in both gaps and the gas has the same velocity, volume flow rate and mass flow rate through the valve opening.
Eq. (12) is solved Y, Eq. (13) is solved for the F_{pl}. This expression depend on the W_2. Eq. (14) is solved for W_2 and Eq. (15) is solved for $\dot{V}(t)$. Eq. (14) depend on the ΔP. Eq. (12), Eq. (13), and Eq. (15) are well known, but this is not the case for Eq. (14). The first and second term on the right hand side originate from the expression for non-steady flow for a frictionsless incompressible fluid:

$$\frac{P_1}{\rho} = \frac{P_2}{\rho} + \frac{W_2^2}{2} + \int_{s_1}^{s_2} \frac{\partial W(s,t)}{dt} ds$$

Here s is a mean streamline through a valve channel, going from point 1 to 2. This expression describes unsteady effects of the Bernoulli equation, in this case gas inertia effects. Using the continuity equation and appropriate assumptions, the integral term is evaluated, resulting in the second term on the right hand side of Eq. (14). For additional information the reader is reffered to [8, 11, 19]
The expression for the pressure difference is given by Eq. (16).

$$\Delta P = P_{suc} - P_{cyl} = P_{suc} - \frac{m}{V_{cyl}} \frac{R}{M_{molar}} T_{cyl} \tag{16}$$

Where m is the mass of the gas in the cylinder, V_{cyl} is the volume of the cylinder, R is the gas constant, M_{molar} is the molar weight of the gas, and T_{cyl} is the temperature in the cylinder. The ideal gas law is used to calculate the pressure in the cylinder. The expression for the mass flow rate is given by Eq. (17).

$$\dot{m} = \rho A_2 W_2 = \rho C_D L Y(t) W_2(t) \tag{17}$$

Recall from Fig. 10 $A_2 = A_L C_D$ where $A_L = LY$.
The volume of the cylinder is calculated using Eq. (18).

$$V_{cyl} = \frac{\pi B^2 \left(L_{rod} + a - acos(\theta) - \sqrt{L_{rod}^2 - a^2 sin(\theta)^2} \right)}{4} \tag{18}$$

Where B is the diameter of the cylinder, L_{rod} is the connection rod length, a is the crank radius, and θ is the crank angle [20].

Now the basic equations needed for setting up the lumped model have been presented. An equation for the valve motion (Eq. (12)), an equation for the gas flow in the valve channel (Eq. (14)), an equation for the pressure difference across the valve (Eq. (16)), an equation for the mass flow rate (Eq. (17)), and finally an equation for the cylinder volume (Eq. (18)). Each of these five equations are investigated individually and some of the assumptions when setting up the lumped model are presented.

3.2.1. Valve Motion Equation

M in Eq. (12) is the sum of the mass of the valve and the equivalent mass of the spring M^*. In order to determine the equivalent mass of the spring theoretically some assumptions are required in order to simplify the problem. The first assumption states the spring is a perfect helical coil, where there are equal distances between each winding. The second assumptions states the total mass is divided into two, where M is the mass of the valve and M^* is the mass of the spring. The third assumption states the free end of the spring (the end connected to the valve) has a displacement Y and a velocity $\dot{Y}$. When an intermediate point of the spring is displaced a distance ξ, the displacement is given by $\frac{\xi}{l}Y$ and the velocity of the equivalent spring mass is given by $\frac{\xi}{l}\dot{Y}$. l is the length of the spring at rest. Fig. 11 illustrates the system.

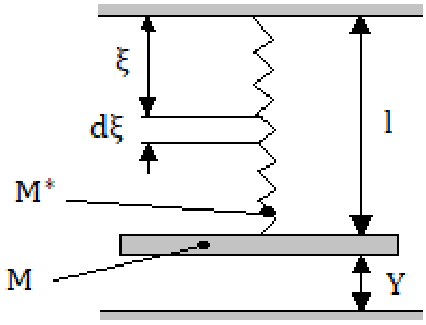

Figure 11: Illustrates the equivalent mass of a spring. Modified from [7]

The kinetic energy of a single element of the spring, with length $d\xi$ is given by Eq. (19).

$$dE_{kin} = \frac{1}{2} dM^* v_{spring}^2 = \frac{1}{2}\frac{d\xi}{l} M^* \left(\frac{\xi}{l}\dot{Y}\right)^2 \tag{19}$$

Thus the kinetic energy of the entire system (valve and spring) is given by Eq. (20).

$$E_{kin} = \frac{1}{2} M\dot{Y}^2 + \frac{M^*}{2l^3}\dot{Y}^2 \int_0^l \xi^2 d\xi = \frac{1}{2}\left(M + \frac{1}{3}M^*\right)\dot{Y}^2 \tag{20}$$

From Eq. (20) it can be seen the mass of the valve and spring is equal to the mass of the valve and an equivalent mass of one third of the mass of the spring. [7] In the model code only the mass of the valve is included, given the spring is a part of the valve.
The flow induced force on the plate is not investigated further in this section regarding the valve motion, only F_0.
Sticktion occurs when there is lubricating oil film between the valve and the valve seat [1]. Sticktion causes an opening delay of the suction valve and may decrease the volumetric efficiency of the compressor, since the gas does not enter the cylinder immediately as the piston moves downward, which is due to the pressure difference across the valve is greater than zero. Sticktion also occurs when the oil film is not present. In an ideal case, the valve would start to open immediately when the pressure in the cylinder is equal to the suction pressure. This is not the case for real applications. In a real case, the pressure difference has to overcome both the spring stiffness and the mass of the valve, before the valve is able to move. The pressure difference across the valve is greater before the valve opens when oil film is present compared to a case without oil film. Lubricating oil film is not included in this thesis. [7] When lubricating oil film is included, the valve opens one degree crank angle after it actually should open. This does not have any significant influence on the lumped model and can therefore be neglected. When setting up CFD models this lubricating oil is very difficult to simulate [3].

3.2.2. Gas Flow

Eq. (14) consist of one term on the left hand side and three terms on the right hand side. The second and third term on the right hand side is investigated in this section regarding the gas flow through the valve channel.

$$\frac{\Delta P(t)}{\rho} = \frac{W_2^2(t)}{2} + J\left[\dot{W}_2(t)Y(t) + W_2\dot{Y}(t)\right] + \frac{c_p A_p W_2(t)\dot{Y}(t)}{2LC_D Y(t)}$$

Both terms account for non-steady flow effects. The second term account for gas inertia and the third term for non-steady work between the valve and the flow.
The gas inertia parameter J depends on valve geometry only and is a dimensionless quantity. The expression for J is given by Eq. (21)

$$J = LC_D \int_{s1}^{s2} \frac{ds}{A(s)} \tag{21}$$

Where $A(s)$ is a varying cross section along a streamline 1-2. The streamline 1-2 is the ideal gas streamline through the valve channel. In the original work by Böswirth, he introduced three parameters accounting for the effect of gas inertia instead of one, namely J which is used in KV-DYN and the lumped model created by the authors. It is possible to use J instead of the original parameters due to three assumptions: the discharge coefficient is not dependent on the valve lift, the discharge coefficient is not affected by inertia effects, and compared to the mass of gas in the seat plate channel, the mass of gas after the 90°-deflection to the effect of gas inertia is small. These assumptions were supported by experimental work and theoretical reasoning [11].
Eq. (21) can be simplified when assuming a constant cross section, $A_p = A(s)$. The new expression for J is given by Eq. (22).

$$J = \frac{LC_D(1 + æd)}{A_p} \tag{22}$$

Where æ is an end correction coefficient with a typical value of 1.4. This coefficient is taking the gas masses accelerated outside the valve channel into account. d is the diameter of the port area.
In KV-DYN, J is not calculated, but based on the users knowledge and experience with gas inertia effects. When setting up the program in MATLAB, J is calculated using Eq. (22), but values provided by [3] is also used. J is typically five when the channel leading to the valve is short. If the channel gets longer, the value of J is also increased. [3]

As mentioned, the third term accounts for non-steady work between the valve and the gas flow. As the valve moves, work is transferred from the gas flow to the valve. This work transfer reduces the velocity of the emerging jet when the suction valve opens. The opposite is true when the valve closes. The specific work exchange between the valve and flow (the third term in Eq. (14)) is obtained by dividing the force acting on the valve with the flow.

When implementing Eq. (14) in the model, $\dot{W}_2$ is solved for. If steady state had been assumed, W_2 is calculated directly from the pressure difference across the valve using

Eq. (23).

$$W_2 = \sqrt{\frac{2\Delta P}{\rho}} \tag{23}$$

Since W_2 is a variable parameter in Eq.(14) this is not possible.

3.2.3. Pressure Difference

Böswirth found that a gas-spring-effect is important. When the valve moves it has a "piston like action" which is considered by the gas-spring-effect. The gas-spring-effect is associated with the displacement of the volume in the cylinder and is therefore included in the expression for P_{cyl}. The gas-spring-effect is not included when calculating the suction pressure, given this pressure is assumed constant.
The gas-spring-effect is needed when valve flutter is taken into account. Flutter is defined as valve oscillations excited by gas forces. This effect is taken into account by introducing a correction coefficient r. The new expression for calculating the pressure in the cylinder is given by Eq. (24).

$$P_{cyl} = \frac{mRT_{cyl}}{V_{cyl} - A_p r Y(t)} \tag{24}$$

Where r is given by the following expression:

$$r = 1 + \frac{D^2 - d^2}{d^2} C_D$$

Here D is the diameter of the valve.
This correction may work like an additional damping force, damping out oscillations, since it creates force pulses which move with the same rhythm as the valve.

3.2.4. Cylinder Volume

In Eq. (18) the angular position (angle domain) is used to calculate the volume of the cylinder. When setting up the model, the motor speed of the compressor should be an adjustable variable, therefore the time domain is preferred. Also, the other basic equations presented are time dependent. The angular velocity, ω, of the crank shaft is assumed constant. When the angular velocity is constant Eq. (25) is valid.

$$\theta = \omega t \tag{25}$$

This term replaces θ in Eq. (18). The expression for ω is given by Eq. (26).

$$\omega = RPM \left(\frac{1}{60} \frac{\text{min}}{\text{s}} \right) \left(\frac{2\pi}{1} \frac{\text{rad}}{\text{rev}} \right) \tag{26}$$

Further, the result of Eq. (25) is given in radians. This is converted to degrees, $1rad = 57.3°$, so the results (e.g. lift height of the suction valve), presented in Sec. 5, are given as a function of degrees crank angle.

3.3. KV-DYN

As mentioned previously, KV-DYN calculates the important dynamic processes for both suction and discharge valves for hermetic refrigeration compressors.
A segment of the assumptions used in KV-DYN when calculating the valve plate movement and the valve flow model are given below:

- The spring force is linear and with precompression
- The valve plate impacts completely inelastic with the valve seat and the limiter
- The gas is considered as compressible in the cylinder, gas flow through the valve is calculated with equations for incompressible fluid
- Isentropic compression and expansion of ideal gas in the cylinder
- Flow- and force coefficient has constant values
- There is a constant suction pressure in the inlet valve plenum chamber
- The gas-spring-effect is taken into account as a coefficient with constant value

Tab. 3 shows the input parameters used to calculate the dynamic processes in KV-DYN.

Table 3: Input parameters KV-DYN

Compressor input parameters	Unit	Valve input parameters	Unit
Valve working pressure	bar	Number of valve units	
Gas density	kg/m^3	Valve port area	mm^2
Isentropic exponent	-	Valve seat area	mm^2
Polytropic exponent	-	Width of sealing land	mm
Pressure ratio	-	Oil sticking crank angle span	$°c.a$
Stroke	mm	Entrance loss coefficient	-
Cylinder diameter	mm	Coefficient for gas-spring effect	-
Piston rod diameter	mm	Gas inertia parameter	-
Clearance volume	%	Valve discharge coefficient	-
Crank radius / conn. rod length	-	Valve plate force coefficient	-
Rel. eccentricity of crank mechanism	-	Valve plate damping coefficient	Ns/m
Compressor speed	min^{-1}	Spring precompression	mm
Specific heat of gas at constant pressure	kJ/kgK	Spring stiffness	N/m
Intake heating factor	-	Mass of valve plate (corr.)	g
Temperature at suction inlet	$°C$	Maximum lift (limiter)	mm

3.4. Assumptions for the Lumped Model

It is assumed the pressure in the inlet plenum chamber is constant, see Eq. (16). It is assumed there is a free flow of gas masses in the inlet plenum chamber. The temperature in the inlet plenum chamber is also constant.
As with KV-DYN, the gas flow through the valve is calculated with equations for incompressible fluid. This is also the case in the cylinder, given that only the dynamics of the suction valve is modelled and the gas is not compressed while the suction valve is open. The effect of expansion is neglected since there is infinite masses of gas capable of flowing into the cylinder from the suction pipeline.
Given that expansion and compression of the gas in the cylinder is neglected, so is the temperature change in the cylinder. The mechanical heat transfer between the piston and the cylinder walls is neglected. Therefore, the temperature in the cylinder is constant and has the same temperature as the gas in the inlet plenum chamber.
As with KV-DYN, the valve impacts completely inelastic with the valve seat and the limiter and the flow- and force coefficient has constant values. Values of the flow - and force coefficient is given by [3]. The gas-spring-effect is taken into account through Eq. (24). Only the mass of the valve is included in the code and not an equivalent mass of one third of the spring mass. It is also assumed that the crank offset moves at constant angular velocity.
The reliability of these assumptions are discussed as the results are presented in Sec. 5 Tab. 4 shows the input parameters needed for the code.

Table 4: Input parameters to the code

Input parameters	Unit
Mass of suction valve	kg
Spring stiffness	N/m
Compressor speed	1/min
Cylinder diameter	m
Connection rod length	m
Crank offset	m
Refrigerant density	kg/m^3
Suction pressure	Pa
Suction/Cylinder temperature	K
Gas constant	kJ/mol K
Port area	m^2
Discharge coefficient	-
Length of seat edge	m
Force coefficient	-
Gas inertia parameter	-
Diameter of flow port	m
Diameter of valve	m

3.5. Implementation to MATLAB

Euler's Method is used as numerical procedure when setting up the model, given it is simpler to set up than the Runge Kutta Method. The basic equations are set up in the order they are solved. In order to illustrate the use of Euler's method, the equation for the valve motion is introduced first, even though the expression is placed last in the code.

A for loop is used to allow the code to be run repeatedly. The equations are placed in the for loop, where the number of iterations, n, are dependent on the time it takes the piston to move θ degrees and the time step size, h. h is determined by the user of the code. The time it takes the piston to move θ degrees is given by Eq. (27).

$$t = \frac{\theta}{RPM}\left(\frac{1}{360}\right)\left(\frac{\text{rev}}{\text{deg}}\right)\left(\frac{60}{1}\right)\left(\frac{\text{s}}{\text{min}}\right) \tag{27}$$

In order to use Euler's method the second order ODE Eq. (12) is reduced into two first order ODE and simultaneous made available for MATLAB. First of all let:

$$Y = Y_1$$

and then let:

$$\dot{Y_1} = Y_2 \tag{28}$$

then Eq. (12) becomes:

$$\dot{Y_2} = \frac{F_{pl}}{M} - \frac{c}{M}Y_2 - \frac{k}{M}Y_1 \tag{29}$$

The second order ODE is reduced into two first order ODE, namely Eq. (28) and Eq. (29) and Euler's method can now be used. The three expressions below calculate the displacement, the velocity, and the acceleration of the valve, respectively.

$$Y_1(n+1) = Y_1(n) + h\dot{Y_1}(n)$$

$$Y_2(n+1) = Y_2(n) + h\dot{Y_2}(n)$$

$$\dot{Y_2}(n+1) = \frac{F_{pl}(n+1)}{M} - \frac{c}{M}Y_2(n) - \frac{k}{M}Y_1(n)$$

3.5.1. Code Setup Approach

Before the results were obtained, some ideas were investigated in order to improve the final code.
Two slightly different codes were modelled in order to investigate the effect of including a clearance volume in the cylinder. The initial conditions and constrains are identical for the two codes, except for the amount of clearance volume. The results where the clearance volume is not taken into account, can be found in App. B.
An issue with respect to the pressure difference across the valve, occurred when the different settings were tested. The initial position of the piston is at TDC, meaning there is no initial pressure inside the cylinder. This leads to the valve moves immediately as the piston move toward BDC. In a real compressor cycle the pressure in the cylinder is equal to the discharge pressure when the piston is at TDC. In order to implement this in the code, expansion of the refrigerant should be taken into account.
Different settings are tested before the final code is run. First, all the initial conditions and the size of the time step is determined. In order to solve the system of equations, an initial condition for the valve displacement is required. Zero can not be used as initial condition. The smallest possible value is used so the code is not terminated. The initial value for the lift height of the valve is $1 \cdot 10^{-5} m$.
The time step size is $1 \cdot 10^{-8} s$. A larger time step terminates the code and a smaller time step increase the computational time without any significant change in the results.

The flowchart given in Fig. 12 shows the order the system of equations are solved in.

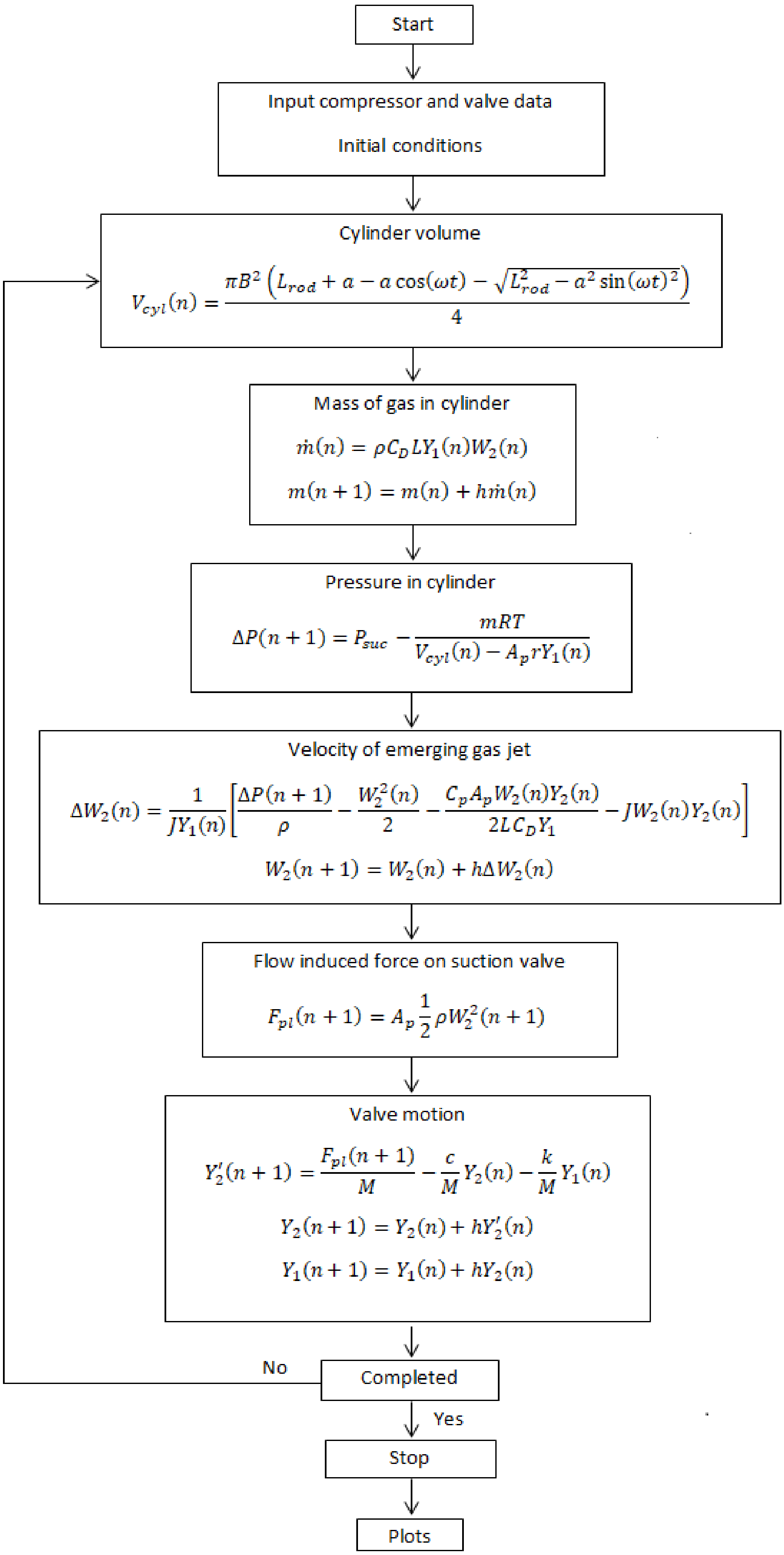

Figure 12: Flowchart of the model

In order to run the code first, compressor and valve data is required. In the same step initial conditions are required. First is the volume of the cylinder calculated at the time t. This step in the code is only dependent on the time step size, whereas the other steps (those including equations) are dependent on each other. The third step calculates the mass of refrigerant in the cylinder. The fourth step calculates the pressure in the cylinder. The fifth step calculates the emerging gas jet velocity. The sixth step calculates the flow induced force on the suction valve. When these steps are completed the valve motion is determined. This procedure continues until the final iteration is reached. When the calculations are completed the code stops and plots three figures: the valve displacement, the velocity of the emerging gas jet, and finally the pressure difference across the valve, all as a function of the crank angle.

4. CFD/FSI Model

In this section the methods used when setting up the 2-D CFD/FSI model is presented. The geometry of the simplified compressor is introduced. A dynamic mesh method accounting for the movement of the valve and the piston is introduced and how to use the method is explained. This method include a "Smoother", a "Remesher", and a "Layering" option. The use of UDFs are introduced, including how to use ANSYS Fluent macros. The 6DOF solver is introduced. This solver is used to specify how many degrees of freedom the valve has. An event mode is also used when setting up the model.
Compressible flow is used for the simulations since a pressure difference is necessary to simulate the fluid structure interaction on the suction valve. Fluid structure interaction is an event where a fluid creates enough force on an object/structure to have the object/structure move or deform/skew. For this simulation only the movement of the structure is of interest and therefore no stress or strain analysis have been performed. To calculate compressible flows the energy equation is enabled. The ideal gas law is used to calculate the density of the gas.

4.1. Geometry

The intend is to implement a 2-D axisymmetric geometry, however, due to difficulties with the dynamic mesh, the problem is simplified, so a 2-D planar geometry is investigated. Some of the problems when using a 2-D axisymmetric geometry is presented in Sec. 4.3
Fig. 13 illustrates the geometry used for the simulations.

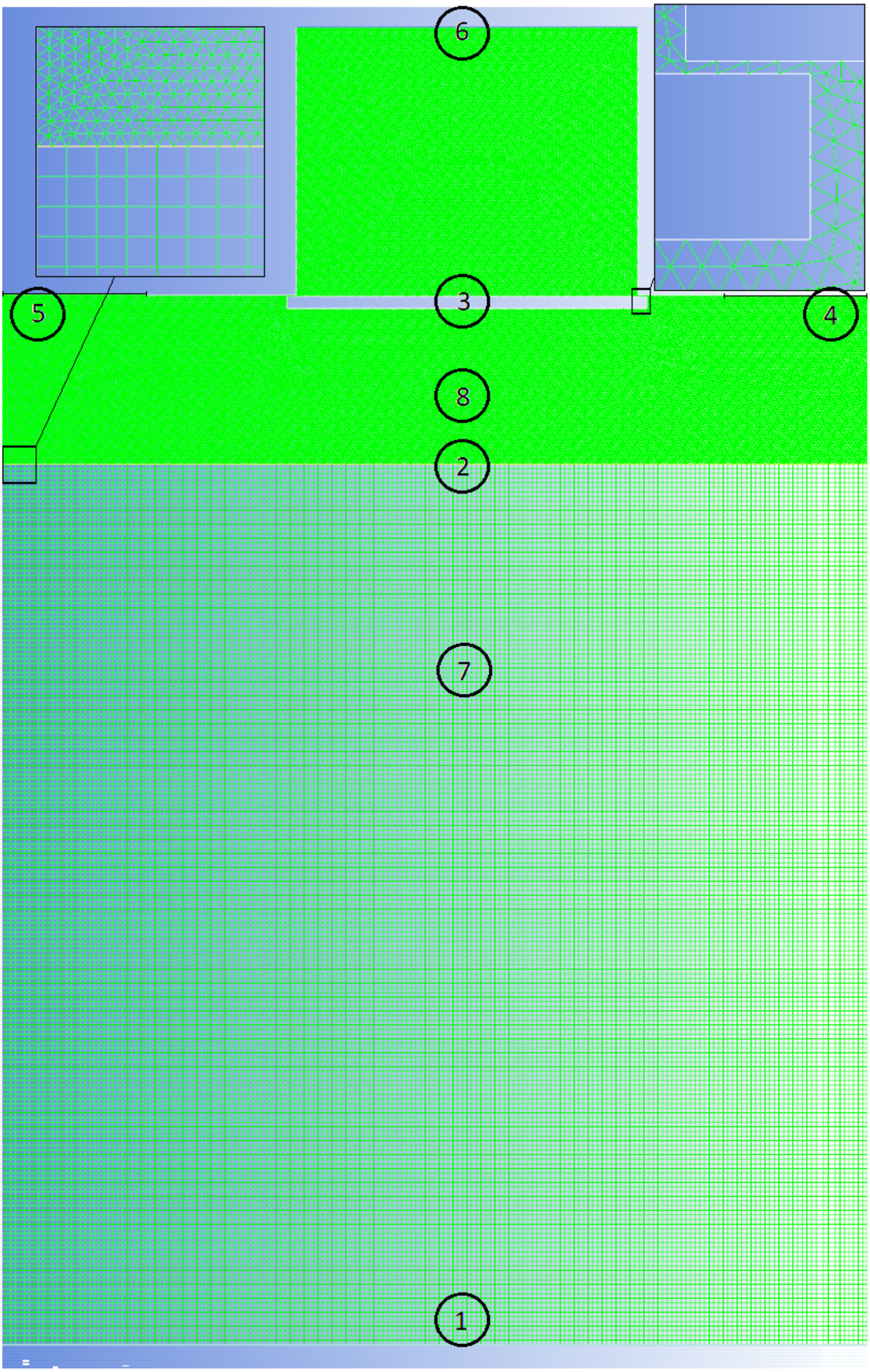

Figure 13: The geometry used for the simulations

Point 1 is where the piston is at BDC. Point 2 is the connection between the piston- and valve chamber, point 7 and 8, respectively. The piston chamber is composed of hexahedral cells and the valve chamber is composed of tetrahedral cells. The reasons for this is explained in Sec. 4.2. Point 3 is the valve. Point 4 and 5 illustrates the two pressure outlets. Point 6 is the pressure inlet.

4.2. Dynamic Mesh

This section is based on the descriptions in ANSYS Fluent's theory- and user guide [21, 22].

For simulations with rigid bodies and moving meshes, the dynamic mesh option in ANSYS Fluent is very useful. It allows rigid bodies to adjust the adjacent cell zones due to the motion defined at the boundaries. Three different methods are available to update the mesh in deforming cell zones: Smoothing, Remeshing and Layering. When boundary displacements are large, it can often result in poor cell quality or the cells can become degenerated. This results in an invalid mesh, e.g. cells with negative cell volume or lead to convergence problems. For the simulations all three options are used. Remeshing and Smoothing are used for the tetrahedral domain and Layering is used for the hexahedral domain. The three options are explained in detail in this section, but first the mathematics behind the dynamic mesh is presented.

4.2.1. Transport Equations

This section is based on the description in ANSYS theory guide [21]. The generic transport equation, when using the dynamic mesh method, is able to take e.g. the turbulence and energy equation into account. Assuming an arbitrary control volume, V, with a moving boundary, the integral form of the conservation equation can be written as Eq. (30). A general scalar, ϕ, is used in the equation.

$$\frac{d}{dt}\int_{v}\rho\phi dV + \int_{\partial V}\rho\phi\left(\vec{u}-\vec{u}_g\right)\cdot d\vec{A} = \int_{\partial V}\Gamma\nabla\phi\cdot d\vec{A} + \int_{V} S_{\phi}dV \tag{30}$$

∂V represents the boundary of the control volume, $\vec{u}$ is the velocity vector, $\vec{u_g}$ is the mesh velocity of the moving mesh, $\vec{A}$ is the area vector, Γ is the diffusion coefficient, and S_ϕ is the source term of the general scalar ϕ.

Depending on what scheme is used to calculate the conservations equations, 1^{st}-order or 2^{nd}-order, the time derivative in Eq. (30) is evaluated differently. When using a 1^{st}-order backward difference approach, the time derivative in Eq. (30) is given by Eq. (31).

$$\frac{d}{dt}\int_{V}\rho\phi dV = \frac{\left(\rho\phi V\right)^{n+1}-\left(\rho\phi V\right)^{n}}{\Delta t} \tag{31}$$

Where n is the respective quantity at the current time step and $n+1$ at the next time level. The time level volume, V^{n+1}, for the $(n+1)$th time is computed using Eq. (32).

$$V^{n+1} = V^{n} + \frac{dV}{dt}\Delta t \tag{32}$$

$\frac{dV}{dt}$ is the volume time derivative of the control volume. When using the dynamic mesh method, the mesh conservation law must be satisfied. The expression for the volume time derivative of the control volume is calculated using Eq. (33).

$$\frac{dV}{dt} = \int_{dV} \vec{u}_g \cdot d\vec{A} = \sum_{j}^{n_f} \vec{u}_{g,j} \cdot \vec{A}_j \tag{33}$$

The number of faces on the control volume is denoted by n_f and $\vec{A}_j$ is the j face area vector. The dot product on the right hand side is calculated using Eq. (34)

$$\vec{u}_{g,j} \cdot \vec{A}_j = \frac{\delta V_j}{\Delta t} \tag{34}$$

δV_j is the volume have been swept out by the control volume face j.

4.2.2. Remeshing

The remeshing method is often used for larger displacements of boundaries compared to the smoothing method. Fig. 14 illustrates how the remeshing method affect the mesh.

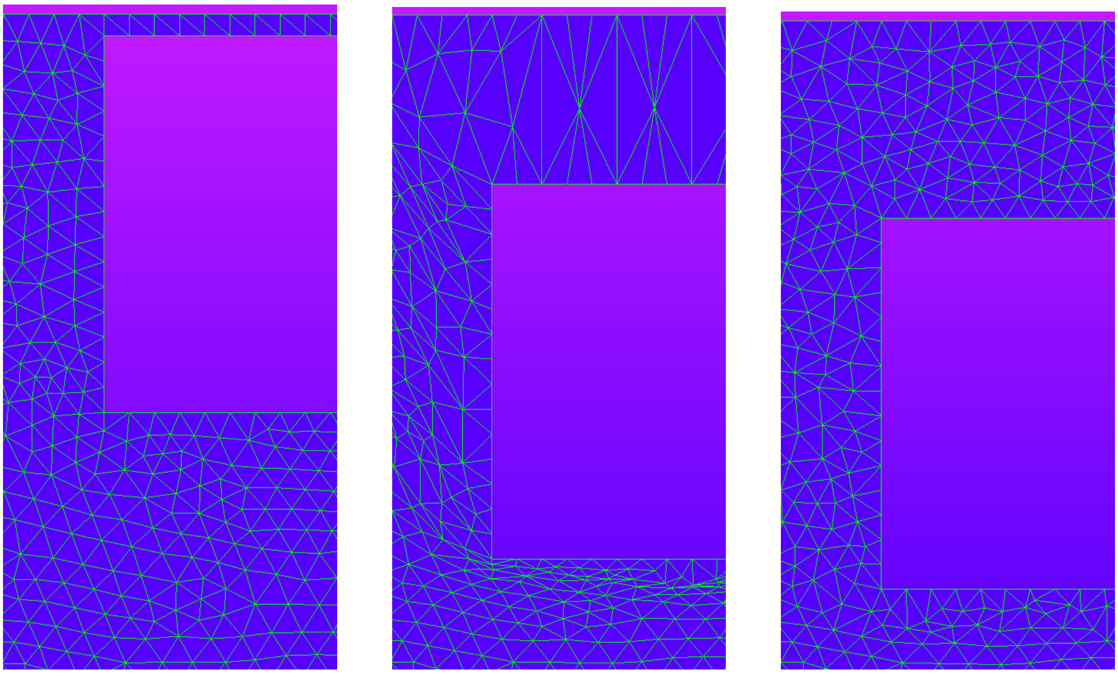

Figure 14: Illustration of the remeshing tool. Left picture: mesh before movement of the valve. Middle picture: mesh just after valve movement. Right picture: the effect of the remeshing tool after valve movement

When a boundary move it often compress the local mesh and results in a cluster of cells that violate the skewness or size criteria given in the meshing tool. The remesher option

automatically replace these compressed cells with new cells interpolated from the old cells, and if these new cells fulfil the skewness criterion, the mesh is locally updated with the new cells. If the cells do not satisfy the criterion they are discarded.
Four different remeshing options is available. Of these only Local remeshing and Face region remeshing support 2-D simulations. These methods only work for triangular-tetrahedral zones. It does also work for mixed zones but here the non-triangular/tetrahedral elements are skipped.
When using Local remeshing method Fluent marks all cells based on their skewness and minimum/maximum length scales. Fluent then evaluates each cell and marks the cell if it does not meet one of the following criteria:

- Greater skewness than the specified
- Smaller than specified minimum length scale
- Greater than specified maximum length scale
- The height does not meet length scale specified for adjacent boundary, e.g. a moving valve

Face regions remeshing helps with remeshing of deformed boundary faces. Fluent marks the deforming faces and based on the minimum and maximum length scale it remeshes the faces and adjacent cells. Both the local and face region remeshing is used for the tetrahedral domain. The skewness is set to be less than 0.7, and the length scale should be between 0.00014 and 0.00016.

4.2.3. Smoothing

The smoothing method includes three different options: the Spring-Based Smoothing Method, the Laplacian Smoothing Method, and the Boundary Layer Smoothing Method. The Remeshing method create new cells due to skewness, the Smoothing method instead applies the change to cell size due to moving boundary to all nodes.
The Spring-Based Smoothing Method use the edges between two mesh nodes as interconnected springs. Equilibrium state is before any boundary motion have occurred. When a displacement happen at a node, it generates a force equal to the displacement between the two nodes. Hooke's law is used to calculate the force between the nodes. This method is used if the movement of the boundary is primarily only in one direction, resulting in no excessive stretching or compression of the cell zone.
The Laplacian Smoothing Method is the simplest smoothing method. This method does not increase the computational requirements significantly, but it does not guarantee improvements on mesh quality. This method adjusts the mesh vertex to the center of the adjacent vertices. This can often lead to poor results, so Fluent only adjusts the vertex to the neighboring vertices if there is an improvement in mesh quality.
The Boundary Layer Smoothing Method is often combined with a mesh motion UDF where the smoothing method is used to deform the boundary layer during the mesh motion.

For the simulations the Smoothing method is used for the tetrahedral domain in combination with the remeshing method. The Spring-Based Smoothing Method is used, since the movement of the valve is only in one direction and no mesh motion UDF is attached to the grid.
When both methods are used simultaneously, they create a strong tool for keeping the mesh refined. The smoothing method is used for when the valve makes small movements. The remeshing method is used for when the valve makes significant movements.

4.2.4. Layering

The layering method lets the user specify an ideal height of the cells adjacent to the moving boundary. This ideal height is then used to either add or remove the layer of cells adjacent to the moving boundary. This method is used for hexahedral and/or wedge mesh zones. The layer (layer j in Fig. 15) next to the moving boundary is split or merged with the next layer (layer i in Fig. 15) of cells based on the height, h, of the cells in layer j.

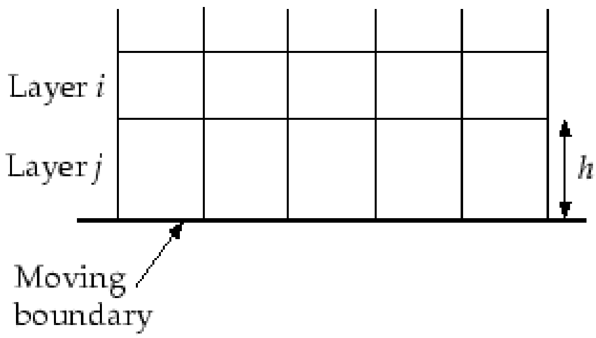

Figure 15: Dynamic mesh Layering method [22]

When the height of layer j is increasing, the layer of cells are kept until:

$$h_{min} > (1 + \alpha_s)h_{ideal}$$

where h_{min} is the minimum cell height of the layer adjacent to the boundary. h_{ideal} is the ideal height, and also the one specified by the user. α_s is the layer split factor. The layer is split into two layers when this condition is satisfied.
Two options are available when using the Layering method: the constant height or the constant ratio. The constant height is where the layer adjacent to the boundary is held constant and the second layer adjacent to the boundary is the one being modified. The constant ratio option lets the Layering method modify the cell layer adjacent to the boundary. [22]
For the simulations layering method is used for the cylinder. The piston chamber consist of hexahedral cells, and the piston only moves in one direction. The constant ratio option

is used, since when the piston reach TDC it only fits one cell, the one adjacent to the piston.

4.3. Troubles with Axisymmetry Geometry

Some of the thoughts and ideas when trying to set up a dynamic mesh for an axisymmetric geometry is explained in this section. Fig. 16 illustrates a simulation where the valve movement was too comprehensive for the dynamic mesh features, and therefore it created several negative cell volumes. To counter comprehensive valve movements a very small time step should be used nor large cell sizes.

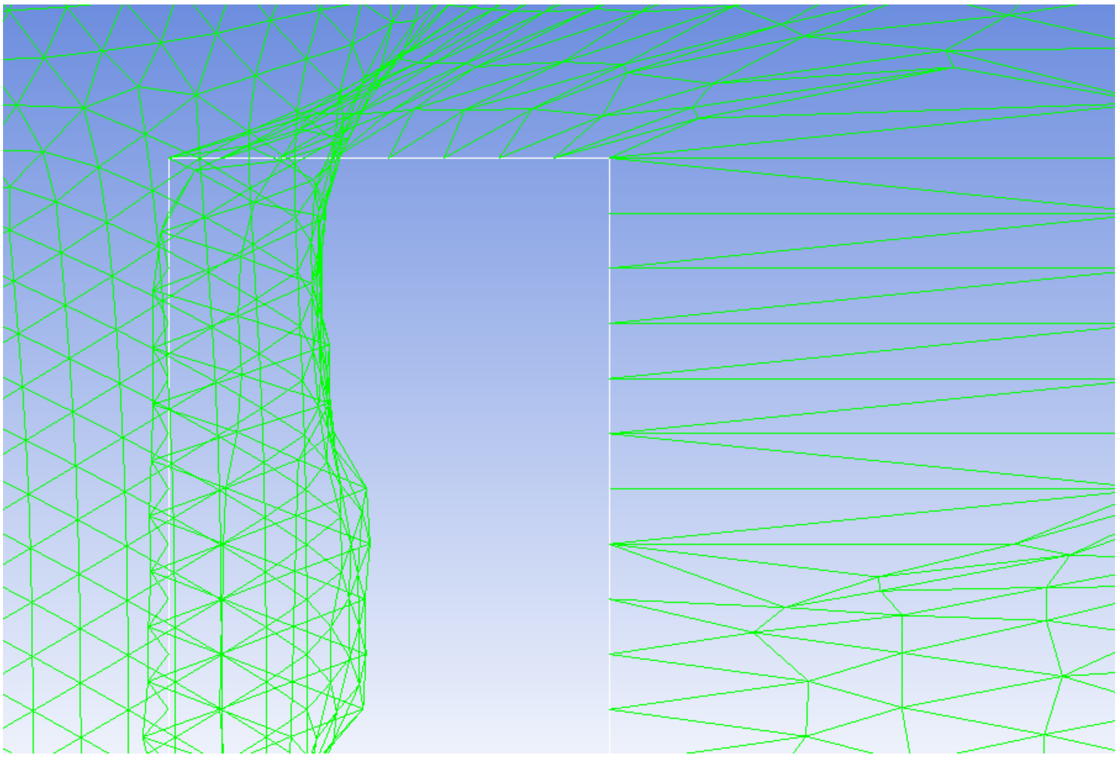

Figure 16: The dynamic mesh were found to have many restrictions for the simulations. Here an illustration of the negative cell volume error is illustrated. This would terminate the simulation

When using both the dynamic mesh and axisymmetric features, other complications occur. Fig. 17 illustrates the axisymmetric geometry intended to use for the CFD simulations. The geometry is divided into two parts, a piston- and valve chamber. For

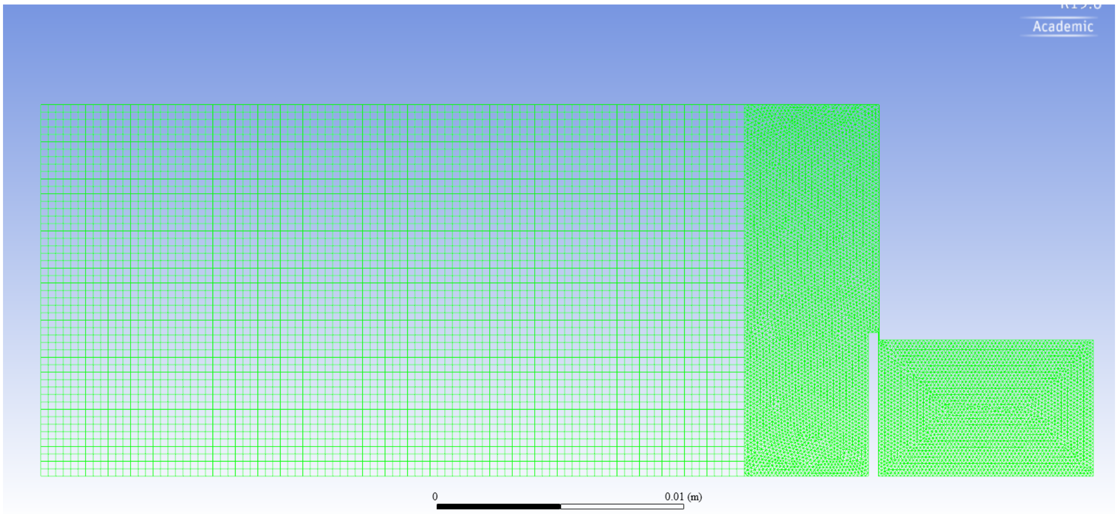

Figure 17: Axisymmetric geometry intended to use for the simulations

the piston chamber hexahedral cells are used and for the valve chamber tetrahedral cells are used. This separation prevents the valve and piston from colliding, which is otherwise possible for an actual compressor. Simulations where all of the geometry are simulated as one domain is performed.
When the whole domain is made of hexahedral cells, the mesh on the side of the valve gives a negative volume when the suction valve moves. This is illustrated in Fig. 18.

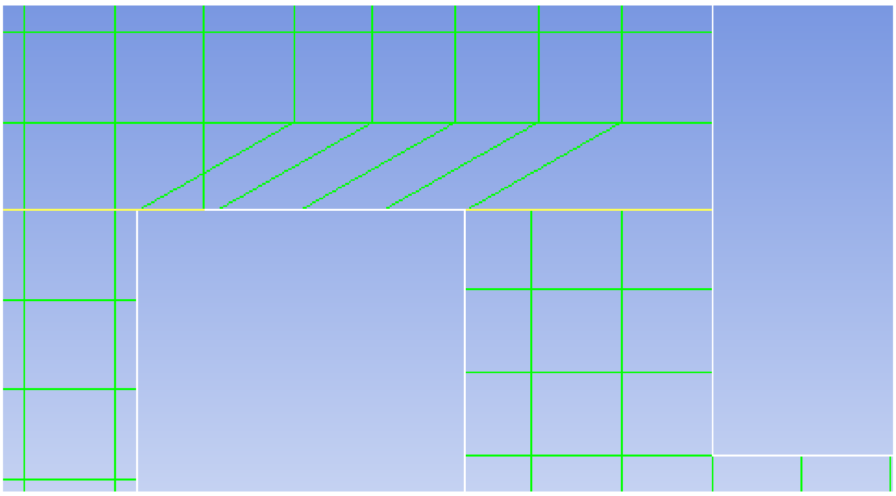

Figure 18: Mesh giving a negative volume at the side of the valve for hexahedral cells

For simulations where the whole domain consist of tetrahedral cells the mesh gave a negative volume at the piston cell nodes and at the axis nodes. This is illustrated in Fig. 19.

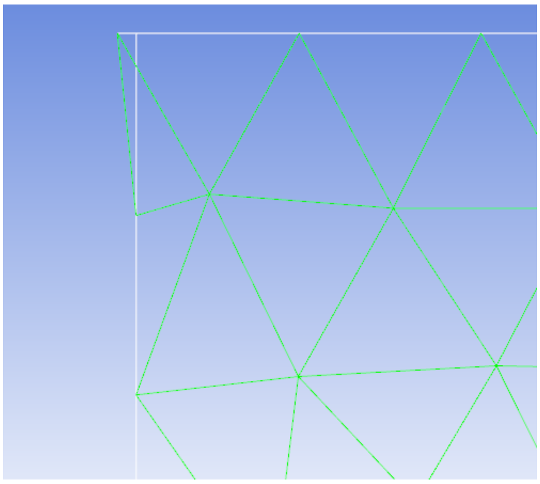

(a) Corner of piston boundary creating a negative cell volume when the piston is moving

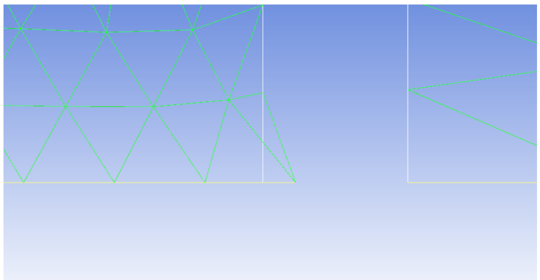

(b) Corner of axis boundary creating a negative cell volume when the suction valve moves

Figure 19: Illustration of negative cell volumes

The test simulations suggests the cell nodes are bound to a specific location on the boundary. For this reason dynamic mesh should be avoided at boundary corners, unless the layering method is used. Though this method is only viable if the moving object is not surrounded by cells. Based on these findings, it is concluded an axisymmetric geometry can not be used for the simulations.

4.4. User Defined Function

UDFs are used to describe functions not yet implemented in ANSYS Fluent. A UDF can either be compiled or interpreted, this is determined by which macros are used in the UDF. When interpreting a UDF ANSYS Fluent does not need additional assistance from programs. When compiling a UDF an external program is used. In this thesis Visual Studio is used. Fluent is run through Visual Studio's command window. Fluent open as normal and is now able to compile the UDF.

4.4.1. Macros

Macros are used to present parameters in ANSYS Fluent and to describe the motion of an object, change in grid or some other function. A macro is read as DEFINE_xx_xxxx and then a paranthesis with the related parameters, velocity, time etc..
The macro "DEFINE_CG_MOTION" is used to describe the motion of the piston. It provides ANSYS Fluent with a velocity for every time step. ANSYS Fluent then translates this to the position of the piston given the current simulation time.

Fig. 20 illustrates the full macro in use.

```
static real velx = 0.0;
DEFINE_CG_MOTION(piston, dt, vel, omega, time, dtime)
{
    NV_S(vel, =, 0.0);
    NV_S(omega, =, 0.0);

    velx = 3.58*sin(261.8*time);
    vel[0]=velx;
    Message ("time = %f, vel[0] = %f\n" , time, vel[0]);
}
```

Figure 20: CG_MOTION macro

Its exact definition is *DEFINE_CG_MOTION(name, dt, vel, omega, time, dtime)*, where *name* defines the name of the UDF. *dt* is a pointer to a storage that contains the dynamic mesh attributes specified by the user or calculated by ANSYS Fluent. *vel* and *omega* is the linear and angular velocities, respectivly. *time* defines the current time and *dtime* defines the time step.
The CG_MOTION macro contains the six arguments mentioned above: *name*, *dt*, *vel*, *omega*, *time*, and *dtime*. These are all variables made by ANSYS Fluent and passed to the UDF. The UDF then calculates the linear and angular velocities and returns the values to ANSYS Fluent.
The CG_MOTION macro have to be executed as a compiled UDF.

4.5. Degrees of Freedom

For the rigid body motion of the suction valve, the 6DOF solver in ANSYS Fluent is used. This solver computes external forces and moments on the valve by computing a numerical integration of the pressure and shear stress over the valve's surface. It can also add additional forces or moments such as e.g. spring forces. When the forces and moments are applied to a valve it calculates the translational and rotational motion of the center of gravity of the valve. The translational motion of the center of gravity of the valve is computed by Eq. (35).

$$\dot{\vec{V}}_G = \frac{1}{m} \sum \vec{F}_G \tag{35}$$

Here $\dot{\vec{V}}_G$ is the translational movement, M is the mass of the valve and $\vec{F}_G$ is the gravitational force vector.

4.6. Event Mode

When setting up the geometry, only the suction valve and the cylinder is included. However, an outlet is needed so the compressed gas can leave the compressor. Event mode for dynamic mesh problems in ANSYS Fluent is used to create a temporary pressure outlet. This pressure outlet is used to simulate a discharge valve. The discharge valve is assumed to be ideal, meaning it is either fully open or fully closed. Reason for this is only the disposal of the refrigerant is of interest.
Using the event mode option, it is possible to define at what time or crank angle an event should happen for transient flows. When the piston is at BDC, the cylinder is filled with refrigerant, and starts to move towards TDC. When a pressure greater than that of the discharge pressure is reached, the pressure outlet is activated. When the piston reaches TDC the pressure outlet is converted to a solid wall, illustrating a fully closed discharge valve.

4.7. Discretization Method

When using the Pressure-based solver a pressure-velocity coupling method is used. Four methods are available: SIMPLE, SIMPLEC, PISO and FSM. The SIMPLE and SIMPLEC algorithms is mainly used for steady state problems, where as the PISO method is mainly for transient flows. For this simulation the SIMPLE pressure-velocity coupling method is chosen. PISO algorithm is practical for larger time step sizes, where as for this simulation small time steps is used, causing the PISO algorithm to be computational expensive. SIMPLEC can improve convergence for uncomplicated simulations with laminar flow, which is not the case for this simulation. FSM is only used when Non-Iterative Time Advancement is chosen.
The solutions methods used for the simulation is illustrated in Tab. 5

Table 5: Solution methods for the simulation

Pressure-Velocity Coupling	
Scheme	SIMPLE
Spatial Discretisation	
Gradient	Green-Gauss Cell Based
Pressure	Second Order
Density	Second Order Upwind
Momentum	Second Order Upwind
Turbulent Kinetic Energy	Second Order Upwind
Turbulent Dissipation Rate	Second Order Upwind
Energy	Second Order Upwind
Transient Formulation	First Order Implicit

As gradient discretisation method the Green-Gauss Cell Based method is chosen. For accuracy the second-order schemes are chosen for every discretisation. Second order is superior compared to the first order schemes for triangular and tetrahedral meshes, which is the mesh type used around the valve. First Order Implicit is chosen for the transient formulation since it is recommended for most problems.
The solution controls used for the simulation is illustrated in Tab. 6.

Table 6: Under-Relaxation Factors used for the simulations

Under-Relaxation Factors	
Pressure	0.4
Density	1
Body Forces	1
Momentum	0.7
Turbulent Kinetic Energy	0.6
Turbulent Dissipation Rate	0.6
Turbulent Viscosity	0.6
Energy	0.7

4.8. Grid Independency Analysis

Data is collected for the valve displacement and the pressure difference across the suction valve for five different mesh sizes. A grid size of 19,920, 35,900, 80,320, 142,142 and 298,000 cells are compared. It should be noted the precise amount of cells change during the simulation. How the values change as the mesh sizes is changed is illustrated in Fig. 21 and 22. Fig. 21 is the valve displacement and Fig. 22 is the pressure difference across the valve.

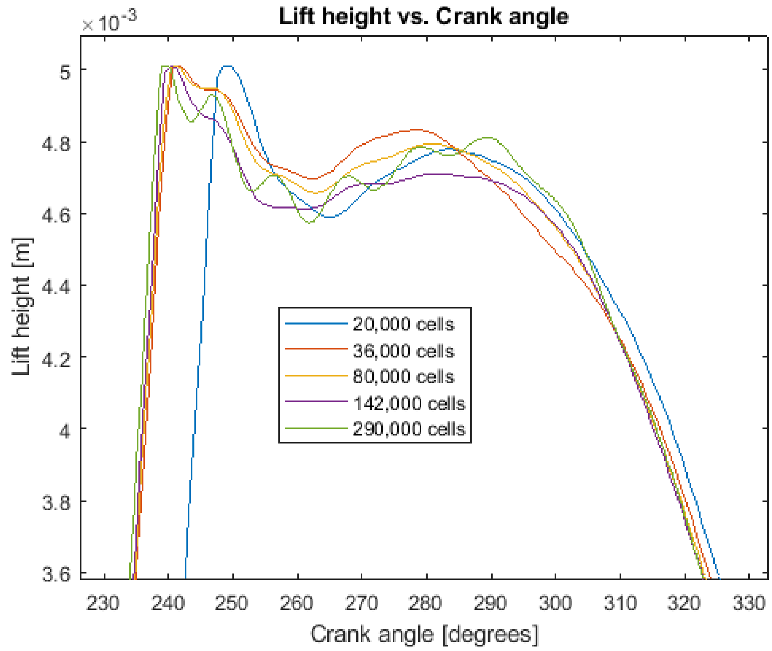

Figure 21: Illustrates the valve displacement for different mesh sizes

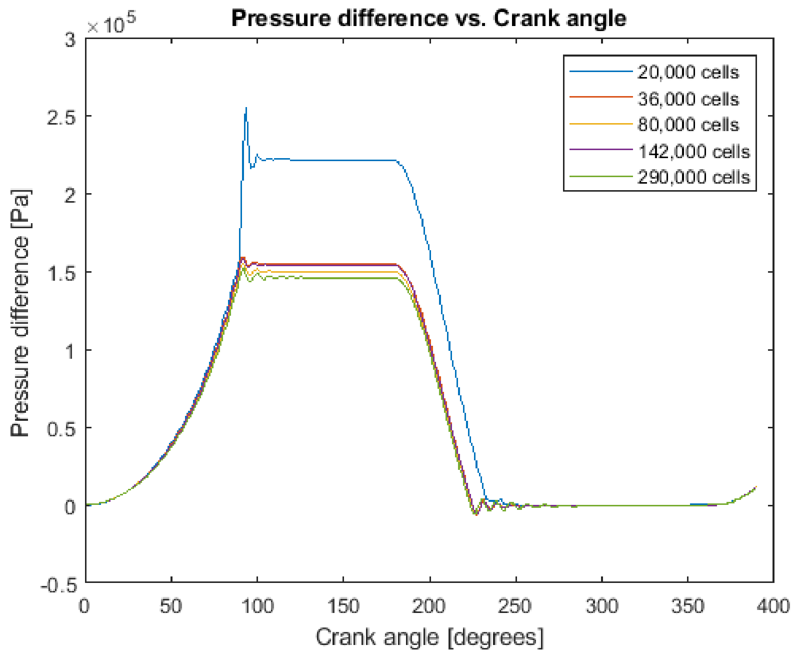

Figure 22: Illustrates the pressure difference across the suction valve for different mesh sizes

The measurements for the valve displacement are very similar, only the simulation with 19,920 cells stand out from the other simulations. The reason for this could be the much larger pressure difference across the suction valve, which have to decrease substantially more to reach a pressure difference of zero or below. The four other simulations have the same tendencies and it is therefore concluded, for the valve displacement and the pressure difference across the suction valve, a grid independency is reached at a grid size of 35,900 cells. The data from this simulation is therefore used for further studies.

4.9. Turbulence Model

The general mass conservation equation and the general momentum conservation equation solved by ANSYS Fluent is given by Eq. (36) and Eq. (37), respectively.

$$\frac{\partial \rho}{\partial t} + \frac{\partial \left(\rho u_i\right)}{\partial x_i} = 0 \tag{36}$$

$$\frac{\partial \rho u_i}{\partial t} + \frac{\partial \left(\rho u_i u_j\right)}{\partial x_j} = -\frac{\partial P}{\partial x_j} - \frac{\partial \tau_{ij}}{\partial x_j} \tag{37}$$

Where P is the static pressure and τ_{ij} is the stress tensor for compressible flow. The expression for the stress tensor is given by Eq. (38).

$$\tau_{ij} = \mu \left[\left(\frac{\partial u_i}{\partial x_j} + \frac{\partial u_j}{\partial x_i} \right) - \frac{2}{3} \frac{\partial u_k}{\partial x_k} \delta_{ij} \right] \tag{38}$$

Where μ is the the dynamic viscosity and δ_{ij} is the Kronecker delta.
Based on a literature study it is decided to use the RNG $k-\epsilon$ turbulence model for solving the flow field. In order to include turbulence in the model, Eq. (36) and Eq. (37) is modified.
The RNG $k-\epsilon$ model is based on Reynolds averaging and Boussinesq's approximation. The variables in the exact Navier-Stokes (NS) equations are decomposed into mean and fluctuating components in Reynolds averaging, e.g. the velocity components:

$$u_i = \bar{u}_i + u_i^{'}$$

Where $\bar{u}_i$ is the mean velocity components and $u_i^{'}$ is the fluctuating velocity components. The same type of expression is also used for other scalar quantities, such as pressure.
Expressions as the one above is substituted into the exact Navier-Stokes equations for continuity and momentum equations and then taking a time average yields the time-averaged momentum equations, also known as Reynolds-averaged Navier-Stokes (RANS) equations. The continuity and momentum RANS equations are given by Eq. (39) and Eq. (40), respectively.

$$\frac{\partial \rho}{\partial t} + \frac{\partial}{\partial x_i} \left(\rho \bar{u}_i\right) \tag{39}$$

$$\frac{\partial}{\partial t} \left(\rho \bar{u}_i\right) + \frac{\partial}{\partial x_j} \left(\rho \bar{u}_i \bar{u}_j\right) = -\frac{\partial \bar{P}}{\partial x_i} + \frac{\partial}{\partial x_j} \left(\bar{\tau}_{ij} - \rho \overline{u_i^{'} u_j^{'}} \right) \tag{40}$$

Where $\bar{\tau}_{ij}$ in this case is the laminar stress and $\rho\overline{u_i^{'}u_j^{'}}$ is the Reynolds stresses. In order to close Eq. (40), the Reynolds stresses must be modelled. This is done using Boussinesq's approach. Boussinesq's hypothesis is the Reynolds stresses are related to the mean flow process and the turbulence is the same in all directions. The expression for the Reynolds stresses is given by Eq. (41).

$$-\rho\overline{u_i^{'}u_j^{'}} = \mu_t\left(\frac{\partial u_i}{\partial x_j} + \frac{\partial u_i}{\partial x_i}\right) - \frac{2}{3}\mu\frac{\partial u_k}{\partial x_k}\delta_{ij} \tag{41}$$

Where μ_t is the turbulent viscosity. The turbulent viscosity depend on the turbulent kinetic energy, k, and its rate of dissipation, ϵ. The expression for μ_t is given by Eq. (42).

$$\mu_t = \rho c_\mu \frac{k^2}{\epsilon} \tag{42}$$

Where C_μ is 0.0845.
The transport equations for the RNG $k-\epsilon$ model is given by Eq. (43) for k, and by Eq. (44) for ϵ, respectively.

$$\frac{\partial}{\partial t}(\rho k) + \frac{\partial}{\partial x_i}(\rho k\bar{u}_i) = \frac{\partial}{\partial x_j}\left(\alpha_k\mu_{eff}\frac{\partial k}{\partial x_j}\right) + G_k - \rho\epsilon - Y_M \tag{43}$$

$$\frac{\partial}{\partial t}(\rho \epsilon) + \frac{\partial}{\partial x_i}(\rho \epsilon\bar{u}_i) = \frac{\partial}{\partial x_j}\left(\alpha_\epsilon\mu_{eff}\frac{\partial \epsilon}{\partial x_j}\right) + C_{1\epsilon}\frac{\epsilon}{k}G_k - C_{2\epsilon}\rho\frac{\epsilon^2}{k} \tag{44}$$

In the two equations, μ_{eff} is the effective viscosity, G_k is the generation of turbulent kinetic energy, and Y_M takes effects of compressibility into account. α_k and α_ϵ are the inverse effective Prandtl number for k and ϵ, respectively. For more information about these terms the reader is referred to ANSYS's theory guide [21]. $C_{1\epsilon}$ and $C_{2\epsilon}$ is 1.42 and 1.68, respectively.

4.9.1. Energy Equation

Given compression is taken into account in the model, the energy equation is solved. The energy equation for heat transport, when taking turbulence into account, is given by Eq. (45).

$$\frac{\partial}{\partial t}(\rho\bar{E}) + \frac{\partial}{\partial x_i}\left[\bar{u}_i(\rho\bar{E} + \bar{P})\right] = \frac{\partial}{\partial x_j}\left(k_{eff}\frac{\partial\bar{T}}{\partial x_j} + \bar{u}_i(\tau_{ij})_{eff}\right) \tag{45}$$

E is the specific energy and k_{eff} is the effective thermal conductivity. $(\tau_{ij})_{eff}$ is the deviatoric stress tensor. The expression for the tensor is given by Eq. (46).

$$(\tau_{ij})_{eff} = \mu_{eff}\left(\frac{\partial u_j}{\partial x_i} + \frac{\partial u_i}{\partial x_j}\right) - \frac{2}{3}\mu_{eff}\frac{\partial u_k}{\partial x_k}\delta_{ij} \tag{46}$$

This term represents viscous heating. μ_{eff} is the total effective viscosity. The total effective viscosity is the sum of the μ and μ_t.

The effective thermal conductivity, when using the RNG $k-\epsilon$ model, is calculated using Eq. (47).

$$k_{eff} = \alpha c_p \mu_{eff} \tag{47}$$

c_p is the specific heat of the refrigerant and α is the thermal conductivity.
The ideal gas law for compressible flows is given by Eq. (48).

$$\rho = \frac{P_{op} + P}{\frac{R}{M_{molar}} T} \tag{48}$$

Where P_{op} is the operating pressure, P is the local static pressure, R is the universal gas constant, M_{molar} is the molar weight of the refrigerant, and T is the temperature. The temperature is calculated from the energy equation.

4.10. Assumptions

The gas is assumed as an ideal gas the density is calculated using the ideal gas law. The ideal gas law states that molecules do not attract or repel each other, and the molecules themselves do not take up volume. This is problematic if the pressure of the gas is maybe hundred times greater than atmospheric pressure or at very low temperatures, e.g. -100°or lower. The operating pressure in the compressor is set to 2.03 *bar* and the temperature of the gas in the suction pipeline is set to 323.15 K, which is acceptable for ideal gas calculations. KV-DYN also use the ideal gas law for compression calculations [14].

For both the lumped model and the CFD/FSI model it is assumed the piston moves at a constant angular velocity.

5. Results and Discussion

This section presents the results from KV-DYN, the model code, and the CFD/FSI model. The results from the model code and the CFD/FSI are discussed as they are presented.

The data in Tab. 7 and Tab. 8 is provided by [3]. These data is for a hermetically sealed reciprocating compressor with a cylinder volume of 20 cm^3. The working refrigerant is propane. Relevant data is used in the lumped model as well as in the CFD/FSI model.

Table 7: Valve Input Data

Valve input data		Unit
Number of valve units	1	-
Valve port area	95.03	mm^2
Valve seat area	95.03	mm^2
Width of sealing land	34.56	mm
Oil stinking crank angle span	0.00	°
Entrance loss coefficient	0.00	-
Coefficient for gas-spring effect	1.00	-
Gas inertia parameter	5.00	-
Valve discharge coefficient	0.50	-
Valve plate force coefficient	1.00	-
Valve plate damping coefficient	0.00	Ns/m
Spring precompression	0.00	mm
Spring stiffness	1700.0	N/m
mass of valve plate (corr.)	0.66	g
maximum lift (limiter)	10.00	mm

Table 8: Compressor Input Data

Compressor input data		
Valve working pressure	2.03	bar
Gas density	3.65	kg/m^3
Isentropic exponent	1.17	-
Polytropic exponent	1.10	-
Pressure ratio	7.55	-
Stroke	28.28	mm
Cylinder diameter	30.00	mm
Piston rod diameter	0.00	mm
Clearance volume	1.50	%
crank radius / conn. rod length	0.200	-
Rel. eccentricity of crank mechanism	0.000	-
Compressor speed	2500	1/min
Specific heat of gas at constant pressure	1.603	kJ/kgK
Intake heating factor	0.800	-
Temperature at suction inlet	50.0	°C

Fig. 23 illustrate the lift of the valve and the pressure difference across the suction valve as a function of the crank angle and Fig. 24 illustrate lift height of the valve and the velocity of the emerging gas jet as a function of the crank angle. In Fig. 23 the valve

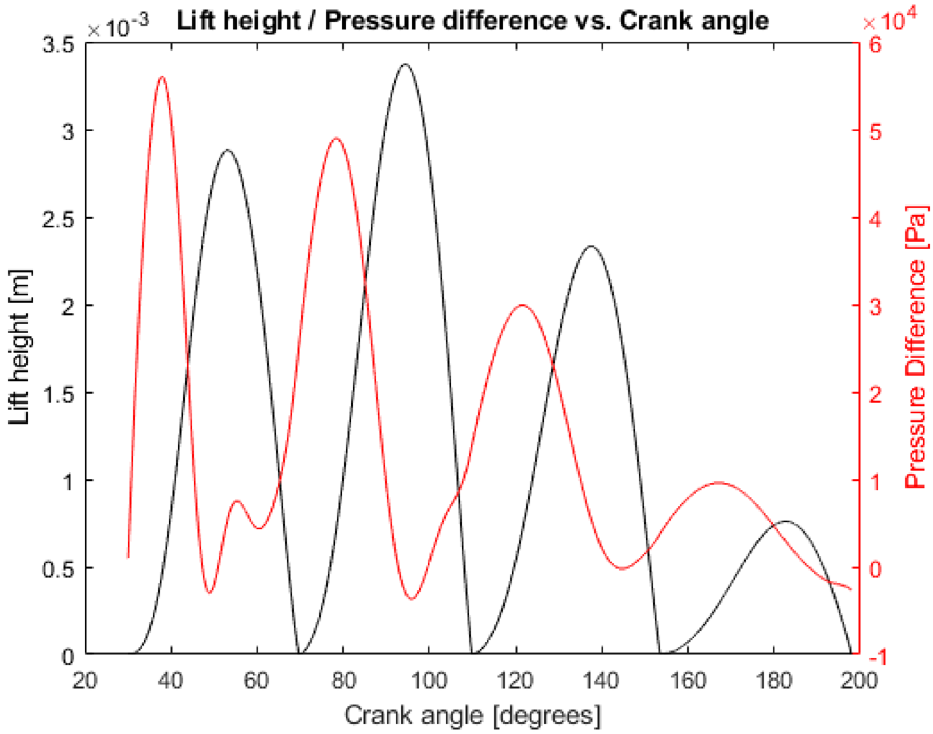

Figure 23: Illustration of the lift height of the valve and the pressure difference across the valve as a function of the crank angle [3]

lift height is given on the left y-axis and the pressure difference across the valve is given on the right y-axis, and the crank angle is given on the x-axis. It can be seen in Fig. 23 the lift height is related to the pressure difference across the valve. As the pressure difference across the valve becomes zero or below the valve starts to open. This happens after approximately 30 degrees crank angle. When the valve is at its maximum lift height the pressure difference across the valve is zero or even negative. As the piston moves toward BDC, the pressure difference across the valve stabilises around zero, meaning the valve once again is closed. This happens after approximately 200 degrees crank angle. As it appear from Fig. 23 the valve is open four times during the suction process (see point 2 and 3 in Fig. 3).

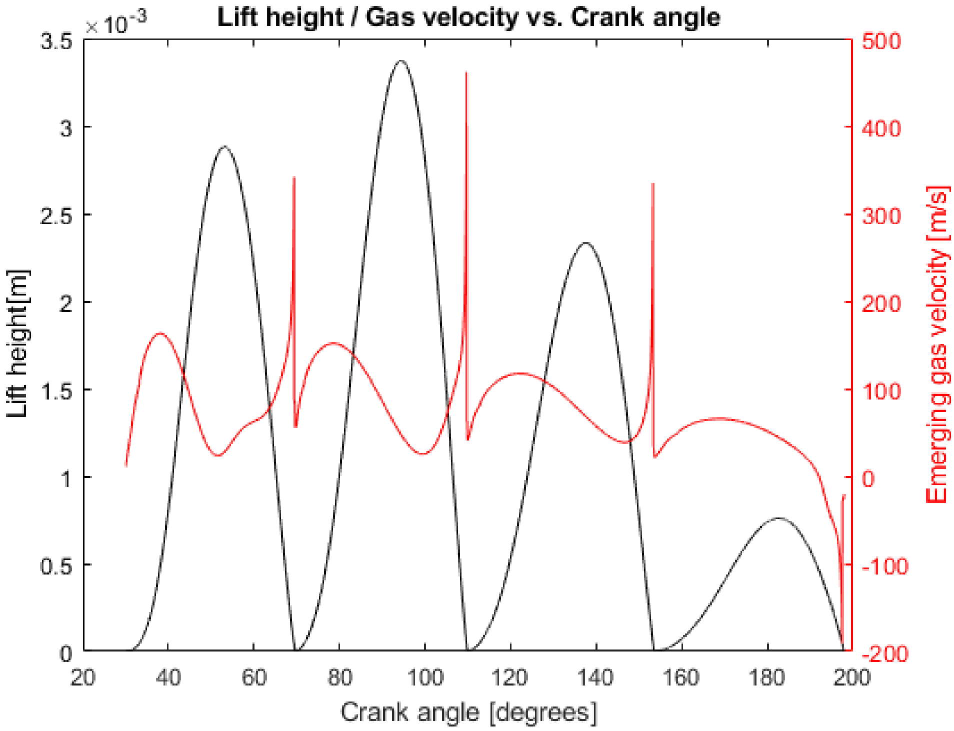

Figure 24: Illustration of the valve displacement and velocity of the emerging gas jet as a function of the crank angle [3]

In Fig. 24 the valve displacement is given on the left y-axis and the emerging gas velocity is given on the right y-axis, and the crank angle is given on the x-axis. It can be seen in Fig. 24 the emerging gas velocity is related to lift height of the valve. As the valve starts to open, the velocity of the refrigerant is accelerated until the lift height of the valve reaches a certain height, then the velocity is decelerated. When the valve is at its maximum lift height the velocity of the refrigerant is at its lowest point and vice versa. When the suction process is completed and the valve is closed, the velocity of the refrigerant becomes negative. This indicates there is back flow, meaning some of the refrigerant exits through the suction valve channel.

From Sec. 4.8 it is determined a grid size of 35,900 cells reach grid independency.

5.2.1. Imagery Illustration of a Piston Revolution

In this subsection a piston revolution is shown through nine images. Fig. 25 illustrates the velocity vectors in the compressor and Fig. 26 illustrates the pressure difference across the valve in contour plots.

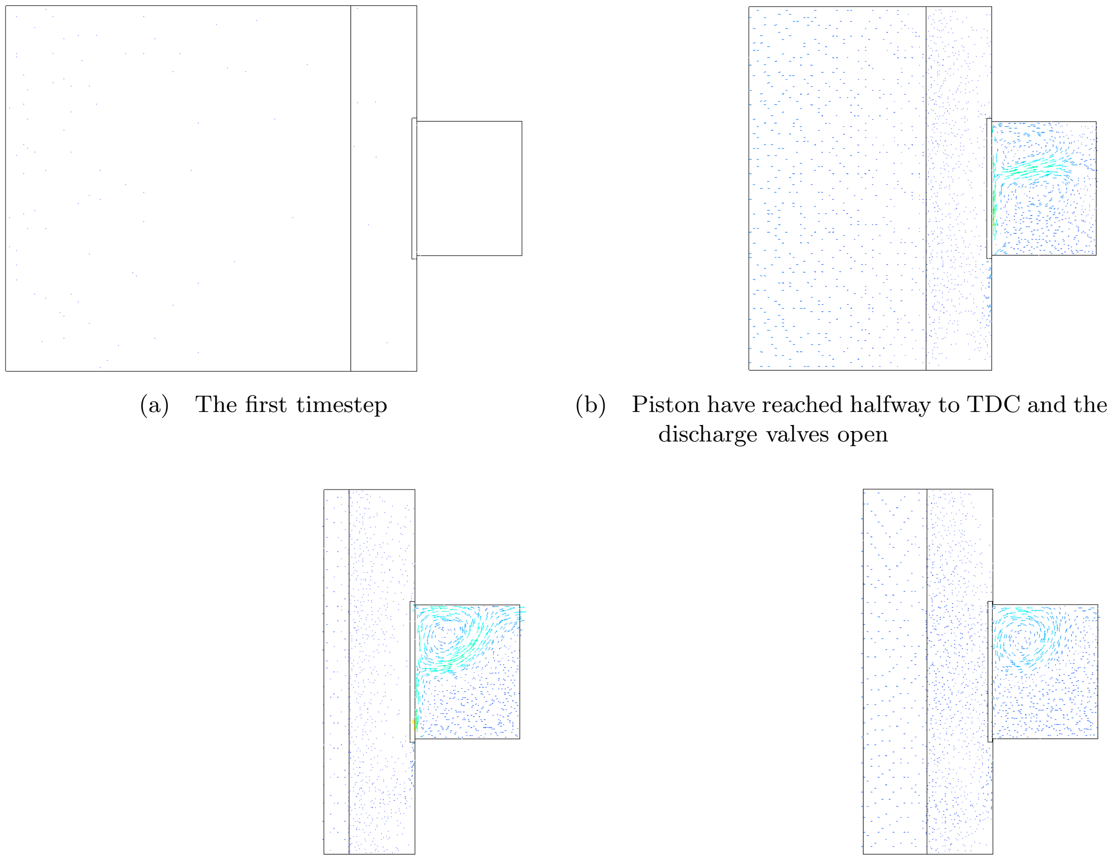

(a) The first timestep

(b) Piston have reached halfway to TDC and the discharge valves open

(c) Piston reach TDC and the discharge valves is again closed

(d) The piston move towards BDC, and at approximately about 226 degrees crank angle the suction valve begins to open

Figure 25: Illustration of the velocity for different degrees crank angle

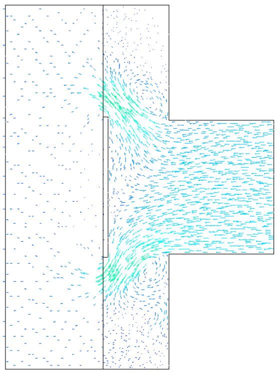

(e) At 240 degrees crank angle the suction valve is at the maximum lift height

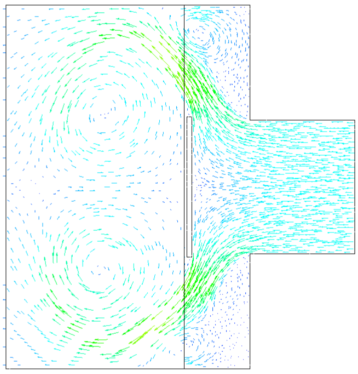

(f) Here the piston is halfway to BDC

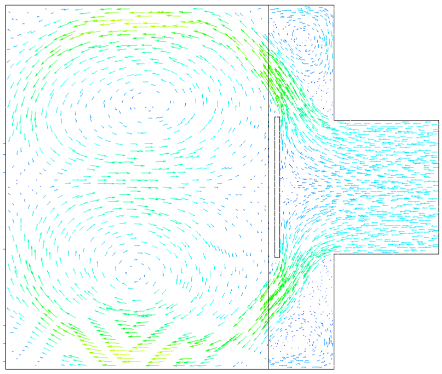

(g) The suction valve has now moved only very little, but now begins to close due to decreasing pressure difference. This happens at 303 degrees crank angle

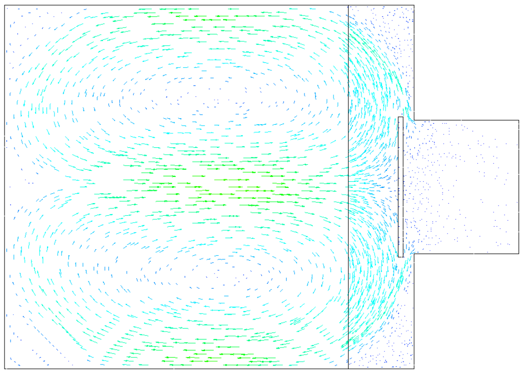

(h) Piston has now reached BDC and completed the revolution

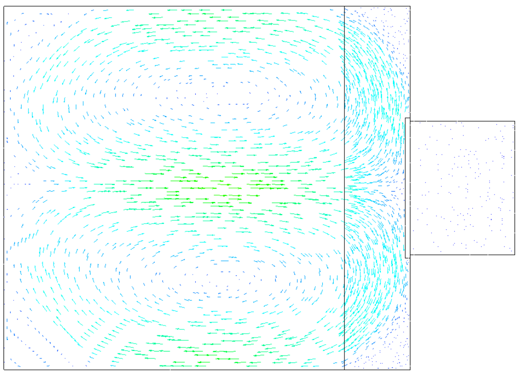

(i) The suction valve is now again fully closed. This happens at 10.8 degrees crank angle for the new revolution

Figure 25: Illustration of the velocity for different degrees crank angle (cont.)

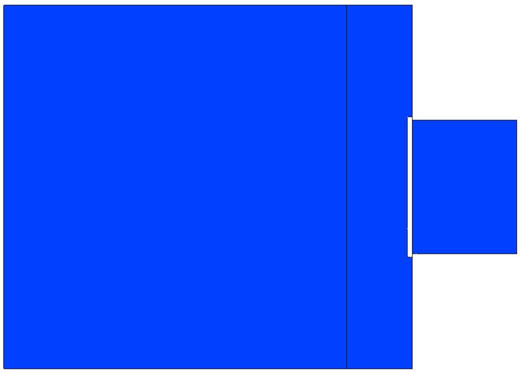

(a) The first timestep. The pressure in the compressor is the defined operating pressure, 2.03 *bar*

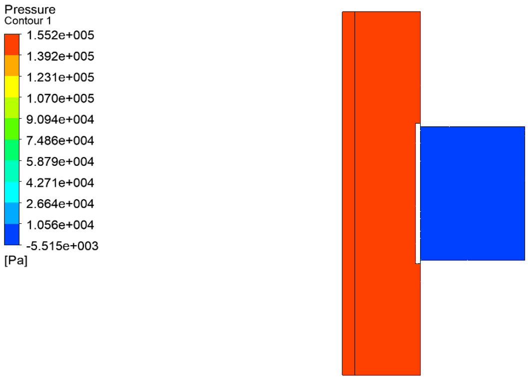

(b) Piston has reached TDC. The compression process is ended

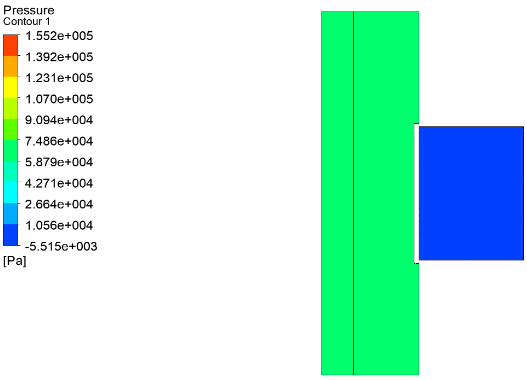

(c) The piston has moved 200 degrees crank angle and the refrigerant is expanding slowly

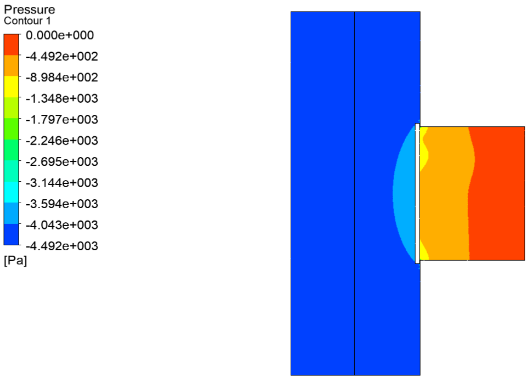

(d) At 226 degrees crank angle the suction valve begins to open. For the next subfigures a local pressure legend will be used instead of a global pressure legend, this is due to only small changes in the pressure difference is happening

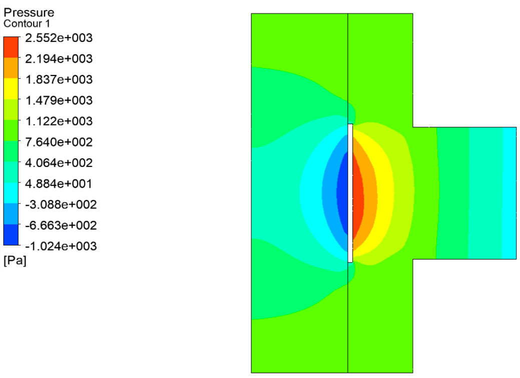

(e) At 240 degrees crank angle the suction is at its maximum lift height

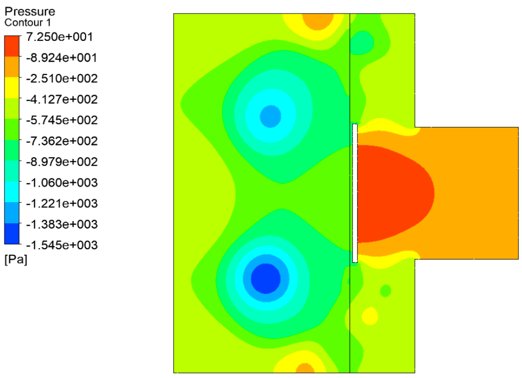

(f) Piston is now halfway towards BDC

Figure 26: Illustration of the pressure difference for different degrees crank angle

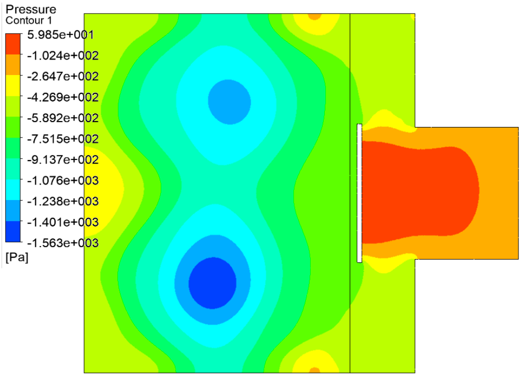

(g) The suction valve now begins to close due to decreasing pressure difference. This happens at 303 degrees crank angle

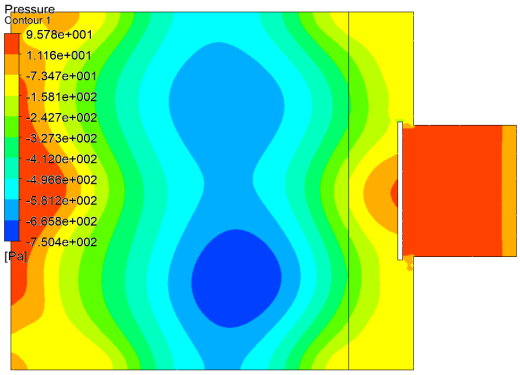

(h) Piston have reached BDC

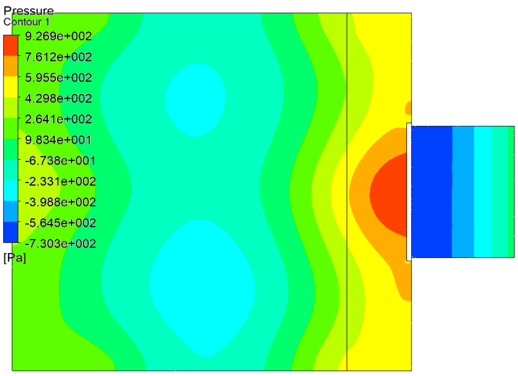

(i) Valve is now fully closed at 10.8 degrees crank angle for the new revolution

Figure 26: Illustration of the pressure difference for different degrees crank angle (cont.)

The raw data from the illustrations above is presented in graphs. The valve displacement and pressure difference across the suction valve as a function of the crank angle is presented in Fig. 27.

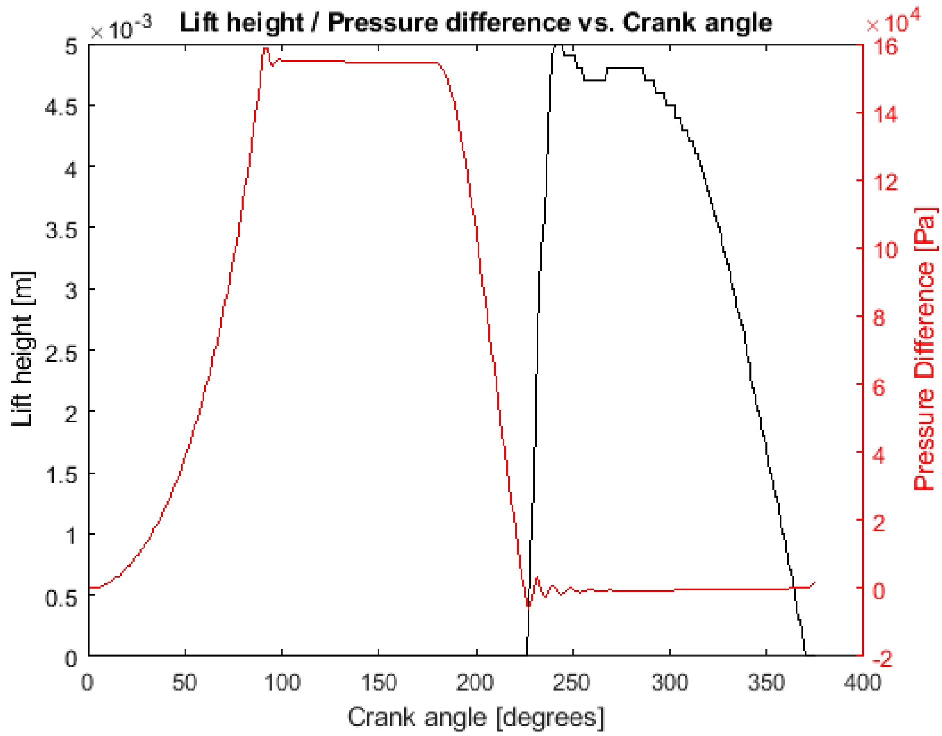

Figure 27: Valve displacement and pressure difference as a function of the crank angle

In Fig. 27, the valve displacement is given on the left y-axis and the pressure difference across the valve is given on the right y-axis, and the crank angle is given on the x-axis. The piston starts at BDC and moves toward TDC. The pressure difference increases until the piston has moved 90 degrees crank angle. Then the discharge valve opens and the pressure in the cylinder stabilises until the piston has reached TDC. As the piston move toward BDC the discharge valve is closed and the refrigerant in the cylinder begins to expand. At 226 degrees crank angle the difference across the valve is able to overcome the spring force and the suction valve starts to open. The suction valve quickly reach its maximum lift height. The valve stabilises at a displacement of 4.6 mm and stays at this lift height. As the piston has reached BDC it starts to move toward TDC again. The pressure difference across the valve is increased and the suction valve is fully closed after approximately 375 degrees crank angle.
Recall Fig. 9 presented in Sec. 3. Fig 27 has the same tendency as the graph in the left bottom corner of Fig. 9. This suggest the CFD/FSI model is able to describe non-steady flow in valve channels.

5.2.2. Comparison of the CFD/FSI Model and KV-DYN

Fig. 28 illustrates the results obtained with the CFD/FSI model and KV-DYN.

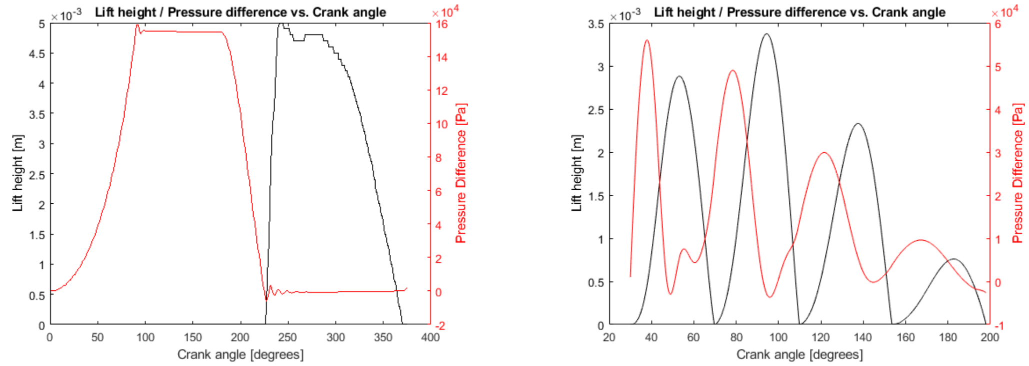

(a) CFD/FSI model (b) KV-DYN

Figure 28: Illustration of the results obtained with the CFD/FSI model and KV-DYN

(a) is the CFD/FSI results and (b) is the results from KV-DYN. The two figures have previously been presented in Fig. 27 and Fig. 23. The two figures are placed side by side in order to clearly show the differences.

It is not appropriate to compare the two different models in exact data, but instead study the tendencies. Many assumptions are made for the lumped model given it is based on experience and semi-empirical equations. The CFD model requires less experience regarding compressor features and the flow field is solved using RANS equations. From the two figures it can be seen the suction valve is displaced as the piston begins to move toward BDC. The is valid for both models. The pressure difference across the valve is also oscillating for both models. The main differences are the amount of oscillations of the suction valve and the degree at which the valve oscillate. Reasons for this disagreement may be explained with the discharge coefficient. The discharge coefficient is used as a constant to describe the effective flow area for the lumped model. It is used in Eq. (17) to calculate the actual mass flow rate through the valve channel. When the discharge coefficient is constant only two variables remain to determine the mass flow rate, the emerging gas velocity and the valve displacement. When the valve is at its maximum displacement the velocity of the emerging gas is low and vice versa. These to both become zero when the valve closes fully. In the CFD model the discharge coefficient changes throughout the compressor cycle. Based on the results presented in Fig. 27 this suggest the discharge coefficient, on average, is greater than the discharge coefficient used in KV-DYN. If the effective area is greater, more gas occupies the valve channel, which may keep the valve open given the spring force can not close the valve. Therefore, the valve first closes when the pressure difference is greater than zero.

The mass of the valve may vary with respect to the valve displacement. This is not taken into consideration. Due to the valve mass change is not thought to vary significantly, but only a very small amount, it is not expected to have any visual effect on the results.

The effect of the spring stiffness is also discussed. The spring stiffness would if decreased, increase the effect of the oscillation of the suction valve. This would make the simulation more realistic, since for actual compressors the suction valve often have several oscillations. The spring stiffness is used from an actual compressor design together with the input parameters presented in Tab. 3.
Another reason for the differences may be the effect of the valve constraint used in the CFD model. The suction valve is constrained to only move 5 mm. The results show the suction valve reach this constrain as the piston move toward BDC, and then stabilise shortly after. If the constrain is removed, the valve would have a greater first oscillation and therefore use more oscillations to stabilise.

5.2.3. Discussion of Results

In this section, limitations, problems, results, and choices are discussed further.

During the setup of the model some adjustments was made due to technical restrictions and time constraints. The intended model should not have had a small gap between the suction valve and the compressor wall. This gap is needed for meshing purposes. The gap creates a small backflow through the suction valve, increasing with the pressure difference. This backflow could be the reason for the lack of pressure build up in the compressor. As appears from Tab. 7 the discharge pressure is 15.33 bar. The model can not reach this pressure and therefore the discharge valve is set to open when the piston has moved 90 degrees crank angle. Here the pressure is read and used as the gauge pressure for the pressure outlet simulating the discharge valve. The pressure in the cylinder then stabilise around the gauge pressure at the discharge valve. When the piston reach 180 degrees crank angle, the discharge valve closes. The refrigerant in the cylinder and clearance volume slowly expands till it reach that of the inlet pressure and overcome the spring force, then the suction valve begins to open.
To avoid mesh difficulties the clearance volume is increased resulting in the piston and suction valve not being able to reach each other. For actual compressors the suction valve is able to hit the piston. This scenario was first intended, but due to remeshing difficulties this was not set up. This also created a constraint for the valve which is not ideal either. First intended the clearance volume should only be 1.5 % of the total compressor volume, but for the simulations a clearance volume of 19 % of the total compressor volume is used.

The code for the lumped model can be found in App. A.
Fig. 29 illustrate the valve displacement and pressure difference across the valve as a function of the crank angle, and Fig. 30 illustrate the valve displacement and the velocity of the emerging gas jet as a function of the crank angle. The results presented are for a cylinder where a clearance volume is taken into account. This is discussed after the presentation of the results.

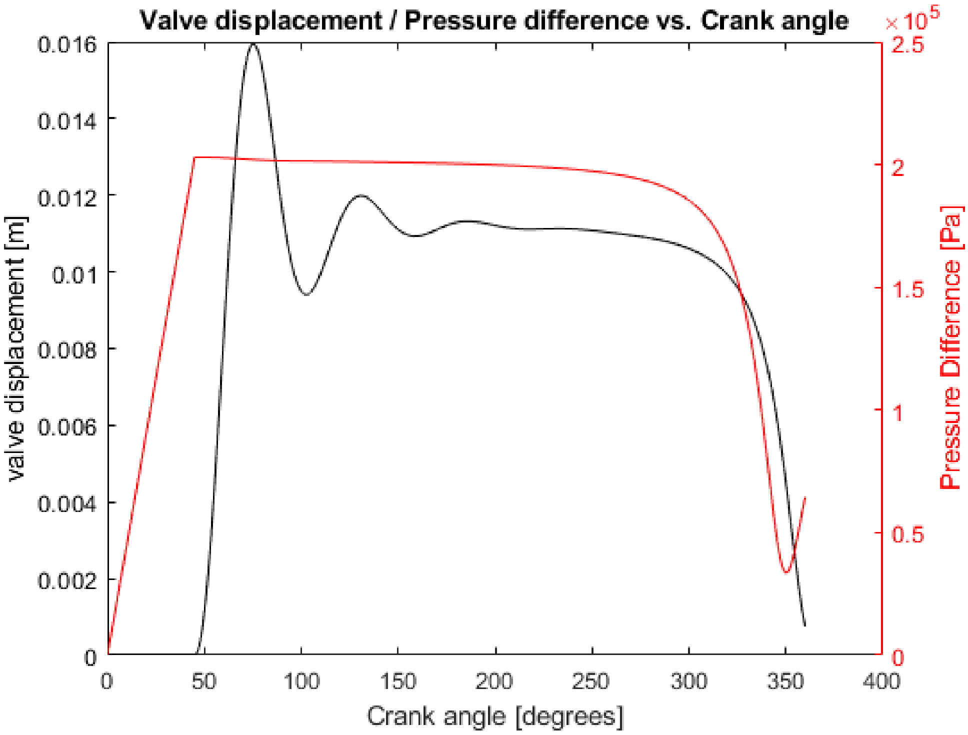

Figure 29: Illustration of the valve displacement and pressure difference across the valve as a function of the crank angle

In Fig. 29, the valve displacement is given on the left y-axis and the pressure difference across the valve is given on the right y-axis, and the crank angle is given on the x-axis. As stated by the system of equations, from the figure it can be seen the valve displacement is dependent on the pressure difference across the valve. When the pressure difference across the valve increases the valve starts to open and the valve stabilises. As the pressure in the cylinder is increased, the pressure difference across the valve approach zero and the valve starts to close again. As mentioned previously, the limiter is not implemented in the program. The valve is displaced 1.6 *cm* from its original position. A displacement of more than 4 *mm* should not possible as given by KV-DYN. This result and the result presented in Fig. 30 does not agree with the results obtained with KV-DYN. See Fig. 23 and Fig. 24. The shape of the valve displacement graph looks familiar. Recall Fig. 9 in Sec. 3. The graph in the left bottom corner describes the valve channel flow. The graph from the code has similar shape as the one presented by Böswirth. This could indicate the code describes the general gas flow through a valve channel.

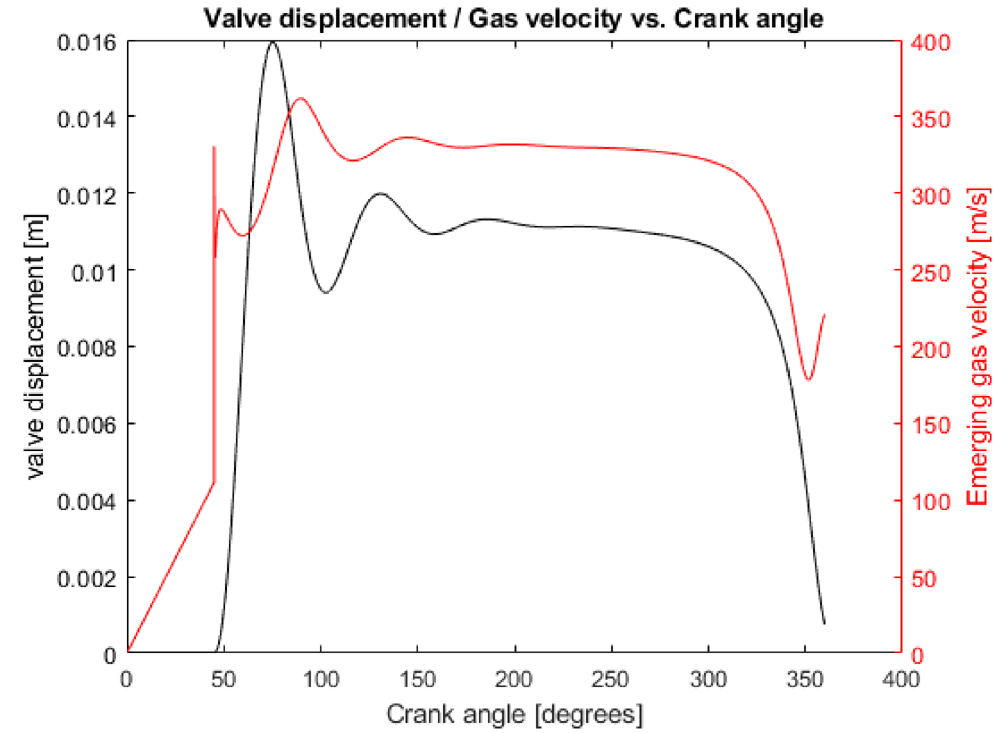

Figure 30: Illustration of the valve displacement and velocity of emerging gas jet as a function of the crank angle

In Fig. 30, the valve displacement is given on the left y-axis and the emerging gas velocity is given on the right y-axis, and the crank angle is given on the X-axis. From Fig. 30 it can be seen the valve displacement is related to the velocity of the emerging gas. As the valve start to open the refrigerant is squeezed out between the newly formed gap. The velocity is then decreased as the valve reach its maximum displacement. When the displacement of the valve is decreased the velocity of the refrigerant is increased and vice versa. This is a correct tendency.

The intend is to solve this problem with the aid of the CFD/FSI results and implementation of constrains in the code. Using the CFD/FSI results from Sec. 5.2, the pressure difference is zero after 0.003 s. This corresponds to a piston motion of 45 degrees crank angle from TDC. This value is implemented into the code, allowing the valve to move when the piston has moved 45 degrees crank angle toward BDC.
The simulation time is determined by how many degrees crank angle the piston is moving from TDC to BDC and back again. Since the response of the suction valve is the only

of interest, the simulation time for an ideal case should only be 180 degrees crank angle, moving from TDC to BDC. This is not an ideal case and therefore the piston begins to move toward TDC before the suction valve close fully. From the data provided by [3] and from the CFD/FSI results, it can be seen the suction valve closes after 17 degrees crank angle and 10.8 degrees crank angle for the new revolution, respectively. The issue with the code is it seems the suction valve closes after roughly 340-360 degrees crank angle. See Fig. 29. Offhand, it seems a factor of two is added somewhere in the code. This is discussed in this section.
A limiter is used in compressors to ensure a maximum valve displacement. This limiter is not included in the code given the valve displacement exceed the maximum possible lift height. When the limiter is included in the code, the valve displacement is at the limited displacement for approximately 320 degrees crank angle. At the remaining degrees of crank angle the suction valve is fully closed. This issue is discussed.

5.3.1. Comparison of Code and KV-DYN

Fig. 31 illustrates the results obtained with the code and KV-DYN.

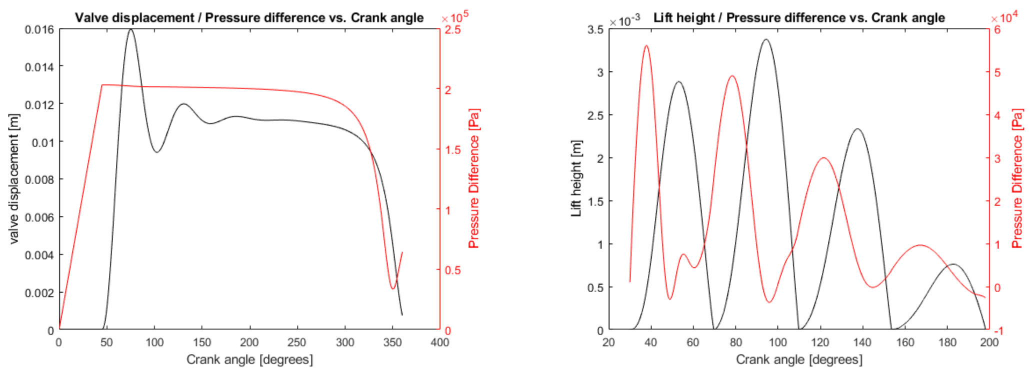

(a) Code (b) KV-DYN

Figure 31: Illustration of the results obtained with the code and KV-DYN

(a) is the code results and (b) is the results from KV-DYN. The two figures have previously been presented in Fig. 29 and Fig. 23. The two figures are placed side by side in order to clearly show the differences.

5.3.2. Discussion of Results

It seems the system of equations are set up in the correct order given the code is able to output results. The results presented in Fig. 29 are taken as the starting point for the discussion. The suction valve does actually close after 360 degrees crank angle. This is due to the pressure in the cylinder. The initial pressure in the cylinder is vacuum, which is not the case in a real compressor. As the valve starts to open, the pressure in the cylinder slowly increases as refrigerant enters. This is a non-physical solution. The

pressure of the refrigerant in the clearance volume remains at the same pressure even though the piston starts to move toward BDC. In a real case the pressure in the cylinder is decreased and the refrigerant occupies the available volume. This is not the case in the code, given the refrigerant is occupying the same volume as it did when the piston was at TDC. In order to solve this problem expansion of the refrigerant must be taken into account.
When the piston move toward TDC, the pressure is increased rapidly after approximately 300 degrees crank angle and the valve closes as the pressure difference becomes zero or negative. This leads to an additional issue. Given only the suction valve is modelled, the refrigerant can not exit the cylinder in any other way than through the inlet plenum chamber. If compression had been implemented in the code, the clearance volume would have been filled with compressed refrigerant. Given this rapid pressure increase is not due to compression, it is necessarily caused by another phenomena. As the piston approaches TDC the refrigerant is trying to exit the cylinder between the suction valve and the port area. The total amount of refrigerant can not be in this gap at the same time. This results in a pressure increase between the suction valve and the piston, creating a large pressure difference resulting in the valve closing.
The idea of locking the valve at its initial position and first allowing it to open when the pressure difference across the valve is zero, does not show any different results compared to when the valve is allowed to move as the piston starts to move. Fig. 32 illustrate the results when the valve is allowed to move immediately as the simulation is started.

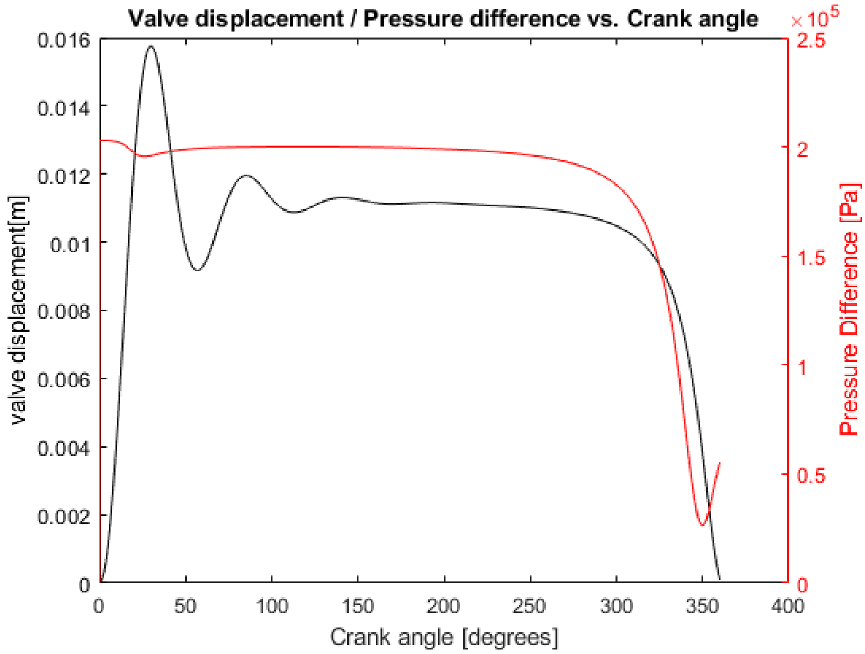

Figure 32: Illustration of the valve displacement and pressure difference across the valve as a function of the crank angle

In Fig. 32, the valve displacement is given on the left y-axis and the pressure difference across the valve is given on the right y-axis, and the crank angle is given on the x-axis. Fig. 32 shows identical results as Fig. 29. The difference between the two results is the results in Fig. 29 is displaced and compressed compared to the results in Fig. 32, meaning the valve closes faster. In Fig. 29 it seems the pressure difference across the valve starts at zero and move toward the maximum pressure difference. This is not the case. The pressure difference is approximately 200,000 Pa from the start of the simulation, which makes sense given the initial pressure in the cylinder is vacuum.
As it can be seen from the presented results, the lift height of the valve is 1.6 cm. This is unrealistic for a compressor/cylinder of the size investigated. The maximum lift height calculated by KV-DYN is approximately 3.4 mm. This issue is once again caused by the pressure difference across the valve. The larger the pressure difference, the larger the valve displacement.
The overall issue with the code is expansion of the refrigerant is not included. The code should have been set up with initial pressure in the cylinder when the piston is at TDC. This pressure should be equal to the discharge pressure and be able to be expanded as the piston move towards BDC. Illustrated in 23 it can be seen the suction valve first is closed after approximately 200 degrees crank angle. This suggest the compression process has started, given the piston is moving toward TDC. Therefore compression should also be included. In order to model the dynamic response of the suction valve the entire compressor cycle should be implemented in the code.

6. Conclusion

The axisymmetric geometry could not be used for the simulations, given the dynamic mesh method was not suited for the investigated geometry.
The 2-D planar CFD/FSI model was able to illustrate non-steady flow in a valve channel, as presented by Bswirth. It is concluded the model is able to simulate the compressor cycle.
The basic non-steady valve flow equations were implemented correct in the code. The lumped model did catch some of the correct tendencies for a compressor, but additional improvements are needed to make the code viable for compressor designs. Too many simplifications were made.
For the results presented in this thesis, it is recommend to use the CFD/FSI model compared to the lumped model. When choosing between a CFD/FSI model and a lumped model, additional research is required. It is expected the two models would be equally viable if the lumped model is to be made with less simplifications and the CFD/FSI model is created in a three dimensional domain.

References

[1] E. L. L. Pereria, C. J. Deschamps, and F. A. Ribas. A Comparative Analysis of Numerical Simulation Approaches for Reciprocating Compressors. *International Compressor Engineering Conference*, 2008. Paper 1879.

[2] M. Costagliola. *Dynamics of a Reed Type Valve*. Phd thesis, Massachusetts Institue of Technology, 1949.

[3] Personal communication, nidec global appliance germany gmbh, 2018.

[4] Bright Hub Engineering. Principle of Working of Refrigeration Reciprocating Compressors. `www.brighthubengineering.com/hvac/51688-principle-of-working-of-refrigeration-reciprocating-compressors/` (online, cited 14.05.18).

[5] Bright Hub Engineering. Parts of the Reciprocating Compressor. `www.brighthubengineering.com/hvac/51899-parts-of-the-reciprocating-compressor/` (online, cited 14.05.18).

[6] R.A. Habing. *Flow and Plate Motion in Compressor Valves*. Phd thesis, University of Twente, 2005.

[7] S. Touber. *A Contribution to the Improvement of Compressor Valve Design*. Phd thesis, Technische Hogeschool Delft, 1976.

[8] L. Böswirth. A Model for Valve Flow Taking Non-Steady Flow into Account, Part I. *International Compressor Engineering Conference*, 1984. Paper 458.

[9] L. Böswirth. A Model for Valve Flow Taking Non-Steady Flow into Account, Part II. *International Compressor Engineering Conference*, 1984. Paper 459.

[10] L. Böswirth. Valve Flow Experiment with Enlarged Models. *International Compressor Engineering Conference*, 1986. Paper 515.

[11] L. Böswirth. Theoretical and Experimental Study on Valve Flutter. *International Compressor Engineering Conference*, 1990. Paper 760.

[12] L. Böswirth. Theoretical and Experimental Study on Valve Flutter, Part II: Flutter Experiments and Similarity. *International Compressor Engineering Conference*, 1990. Paper 761.

[13] L. Böswirth. Non Steady Flow in Valves. *International Compressor Engineering Conference*, 1990. Paper 759.

[14] L. Böswirth. A New Valve Dynamics Simulation Program and Its Use for the Design of Valves. *International Compressor Engineering Conference*, 1990. Paper 1133.

[15] F.F.S. Matos, A.T. Prata, and C.J. Deschamps. Numerical Simulation of the Dynamics of Reed Type Valves. 2002.

[16] E. Kreyszig. *Advanced Engineering Mathematics*. Wiley, 10td ed. edition, 2011.

[17] R. E. Blake. Basic Vibration Theory, 2010.

[18] J. Mayer, P. Bjerre, and F. Brune. A Comparative Study of Different Numerical Models for Flapper Valve Motion. *International Compressor Engineering Conference*, 2014. Paper 2309.

[19] W. W. Heubsch B. R Munson, T. H. Okiishi and A. P. Rothmayer. *Fluid Mechanics*. Wiley, 7td ed. edition, 2013.

[20] MathWorks. Modeling the Motion of an Automotive Piston. `se.mathworks.com/products/demos/symbolictlbx/Piston_modeling/Piston.html(online,cited14.05.18)`,.

[21] Inc. ANSYS. *ANSYS Fluent Theory Guide*, 17.2 edition, 2016.

[22] Inc. ANSYS. *ANSYS Fluent User's Guide*, 17.2 edition, 2016.

Appendix

A. Code used to Generate the Lumped Model Results

```
clc
clear all
close all

%% Valve Properties

M = 0.00066; % Mass of valve [kg]
k = 1700; % Spring constant [N/m]
c = 0; % Damping Coefficient [Ns/m]
%% Cylinder properties
RPM = 2500; % Motor speed [1/min]
omega = (2*pi*RPM)/60; % Angular velocity of crankshaft [rad/s]
b = 0.03; % Bore length of cylinder [m]
l = 0.070; % Connecting rod length [m]
a = 0.01414; % Crank ofset [m]
P_suc = 203000; % Suction pressure [Pa]

%% Gas properites
rho_gas = 3.65; % Density of Propan [kg/m^3]
T = 323; % Temperature in cylinder [K]
R = 0.08149; % gas constant [kJ/mol*K]
M_gas = 0.0441; % Molar weight of Propan [kg/mol]

%% Geometry properties;
A_p = 0.00009503; % port area - constant value [m^2]
C_D = 0.5; % Discharge coefficient [-]
L = 0.03456; % Length of seat edge [m]
C_p = 1; % Force coefficient [-]
J = 5; % Gas inertia parameter [-]
d = 0.011; % Diameter of flow port [m]
D = 0.0117; % Diameter of valve [m]
r = 1+((D^2-d^2)/d^2)*C_D; % Cylinder diameter correction coefficient [-]

%% Setting the time step
t_final = 360/(6*RPM); % Simulation time [s]
h = 0.0000001; % Step size [s]

%% Initial conditions valve
y_0 = 0.00001; % Valve lift height [m]
y_1 = y_0;
```

```
y_0_prime = 0; % Valve velocity [m/s]
y_2 = y_0_prime; % Valve acceleration [m/s^2]
y_2_prime = 0;

%% Initial conditions flow induced force
W_2_0 = 0; % Emerging gas velocity [m/s]
m_gas_0 = 0.0; % Mass of gas in the cylinder [kg]


%% System of equations
n = 1;
for t = 0.0:h:t_final
  if n==1 % Inplementation of inital conditions in the for loop
      y_2(n) = y_0_prime;
      y_1(n) = y_0;
      W_2(n) = W_2_0;
      m_gas(n) = m_gas_0;
    end

    if t <= 0.003 % The valve cant move for the first 0.003 seconds of the simulation
        y_1(n)=0.00001;
      else


        %% Cylinder volume
        V_cyl(n+1) = 9*10^-7+(pi*b^2*(l+a-a*cos(omega*t)-sqrt(l^2-a^2*sin(omega*t)^2)))/4;


        %% Mass flow

        m_dot(n+1) = (rho_gas*C_D*L*(y_1(n))*(W_2(n)))*h;
        m_gas(n+1) = m_gas(n) + m_dot(n);

        %% Pressure difference across the valve

        Delta_P(n+1) = P_suc - (m_gas(n+1)*R*T)/(V_cyl(n+1)-A_p*r*y_1(n));
        %end

        P_cyl(n+1)=(m_gas(n+1)*R*T)/(V_cyl(n+1)-A_p*r*y_1(n));


        %% Gas flow through the valve channel

        Delta_W2(n) = (1/(J*(y_1(n))))*((Delta_P(n+1)/rho_gas)-((W_2(n)^2)/2)-((C_p*A_p*(W_2(n))*
```

```
J*(W_2(n))*(y_2(n)));
            W_2(n+1) = W_2(n)+h*Delta_W2(n);

            %% Flow induced force on the valve plate

            F_pl(n+1)=A_p*0.5*rho_gas*(W_2(n+1)^2);

            %% Valve motion


            y_2_prime(n+1) = (F_pl(n+1)/M) - ((c/M)*y_2(n)) - ((k/M)*y_1(n));
            y_2(n+1) = y_2(n)+h*y_2_prime(n);
            y_1(n+1) = y_1(n)+h*y_2(n+1);

            %% Used for plotting

               n = n+1;
               time(n) = t;
            end
         end

         %% Plotting

         omega = (2*pi*RPM)/60;
         deg = 57.2957; % Degrees per radian
         crankshaft = omega*deg; % Convert from radins to degrees

         figure(1) % Valve displacement
         plot(time*crankshaft,y_1)
         xlabel('Crank angle [degrees]')
         ylabel('valve displacement[m]')

         figure(2) % Pressure difference across valve
         plot(time*crankshaft,Delta_P)
         xlabel('Crank angle [degrees]')
         ylabel('Pressure Difference [Pa]')

         figure(3) % Velocity of emerging gas jet
         plot(time*crankshaft,W_2)
         xlabel('Crank angle [degrees]')
         ylabel('Velocity of emerging jet [m/s]')

         fig = figure;
         left_color = [.0 .0 0];
```

```
right_color = [1 .0 .0];
set(fig,'defaultAxesColorOrder',[left_color; right_color]);
yyaxis left
plot(time*crankshaft,y_1)
title('Valve displacement / Pressure difference vs. Crank angle')
xlabel('Crank angle [degrees]')
ylabel('valve displacement [m]')
yyaxis right
plot(time*crankshaft,Delta_P)
ylabel('Pressure Difference [Pa]')

fig = figure;
left_color = [.0 .0 0];
right_color = [1 .0 .0];
set(fig,'defaultAxesColorOrder',[left_color; right_color]);
yyaxis left
plot(time*crankshaft,y_1)
title('Valve displacement / Gas velocity vs. Crank angle')
xlabel('Crank angle [degrees]')
ylabel('valve displacement [m]')
yyaxis right
plot(time*crankshaft,W_2)
ylabel('Emerging gas velocity [m/s]')

fig = figure;
left_color = [.0 .0 0];
right_color = [1 .0 .0];
set(fig,'defaultAxesColorOrder',[left_color; right_color]);
yyaxis left
plot(time*crankshaft,Delta_P)
title('Pressure difference / Gas velocity vs. Crank angle')
xlabel('Crank angle [degrees]')
ylabel('Pressure Difference [Pa]')
yyaxis right
plot(time*crankshaft,W_2)
ylabel('Emerging gas velocity [m/s]')
```

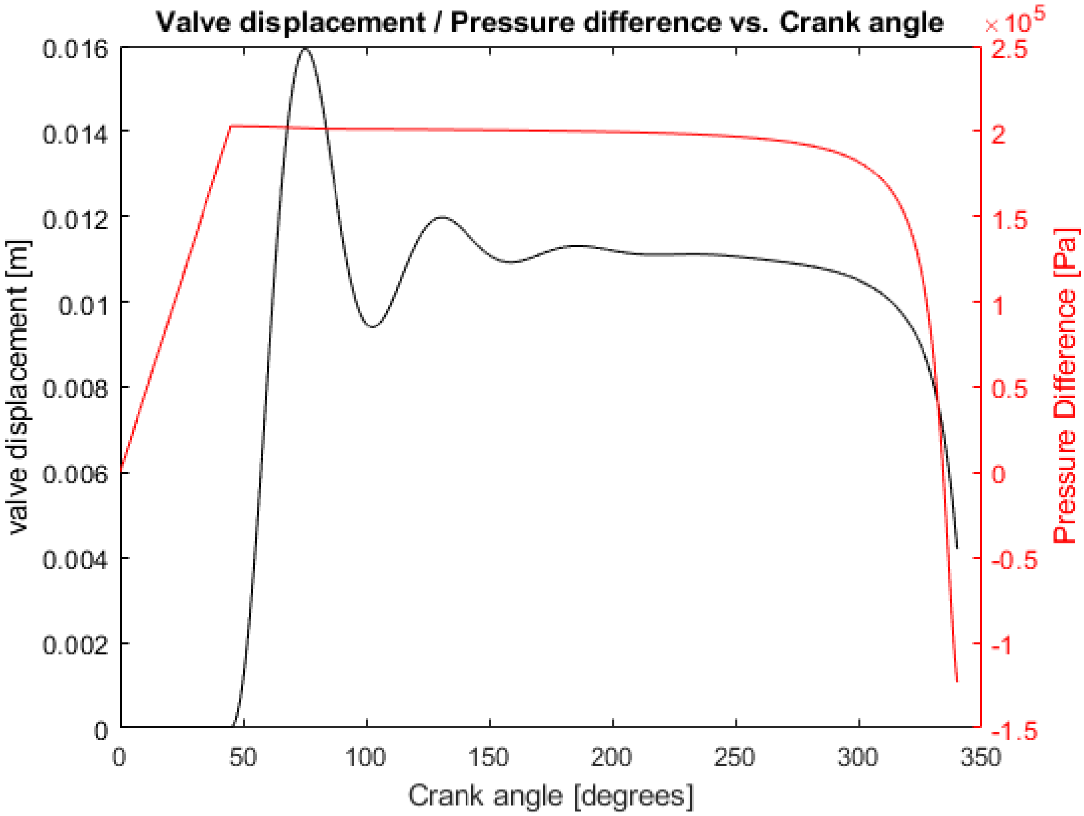

Figure B.1: Illustration of the valve displacement and pressure difference across the valve as a function of the crank angle

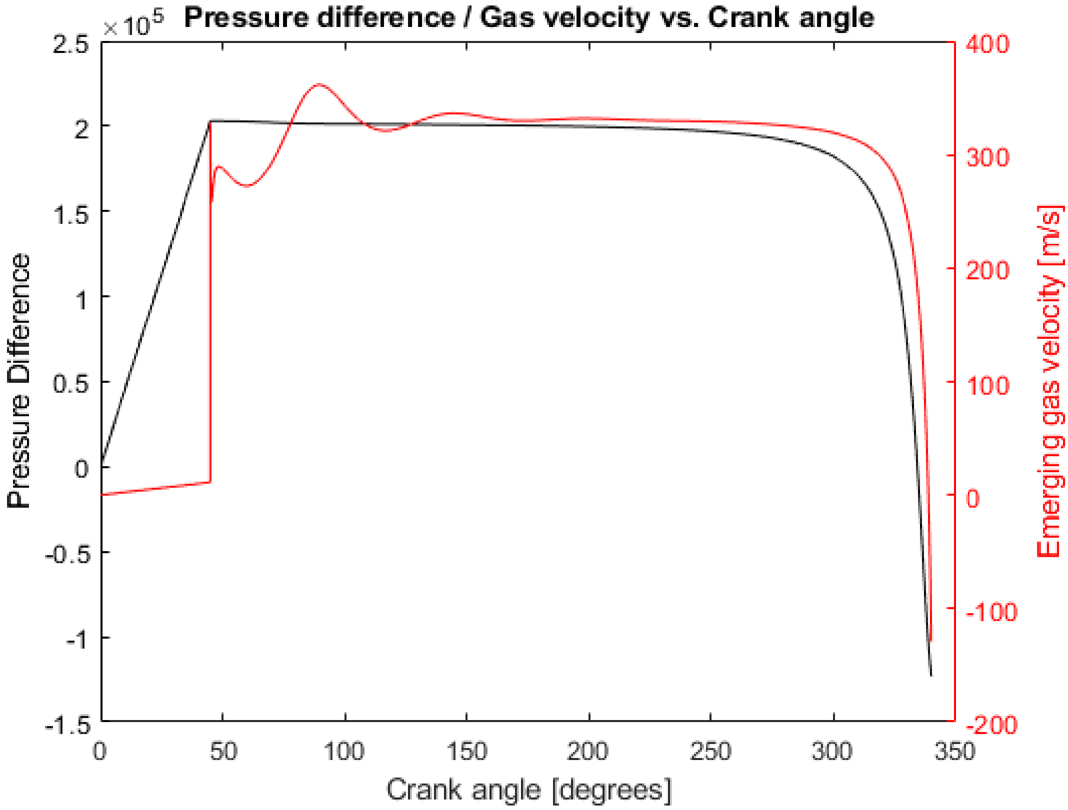

Figure B.2: Illustration of the pressure difference across the valve and velocity of emerging gas jet as a function of the crank angle

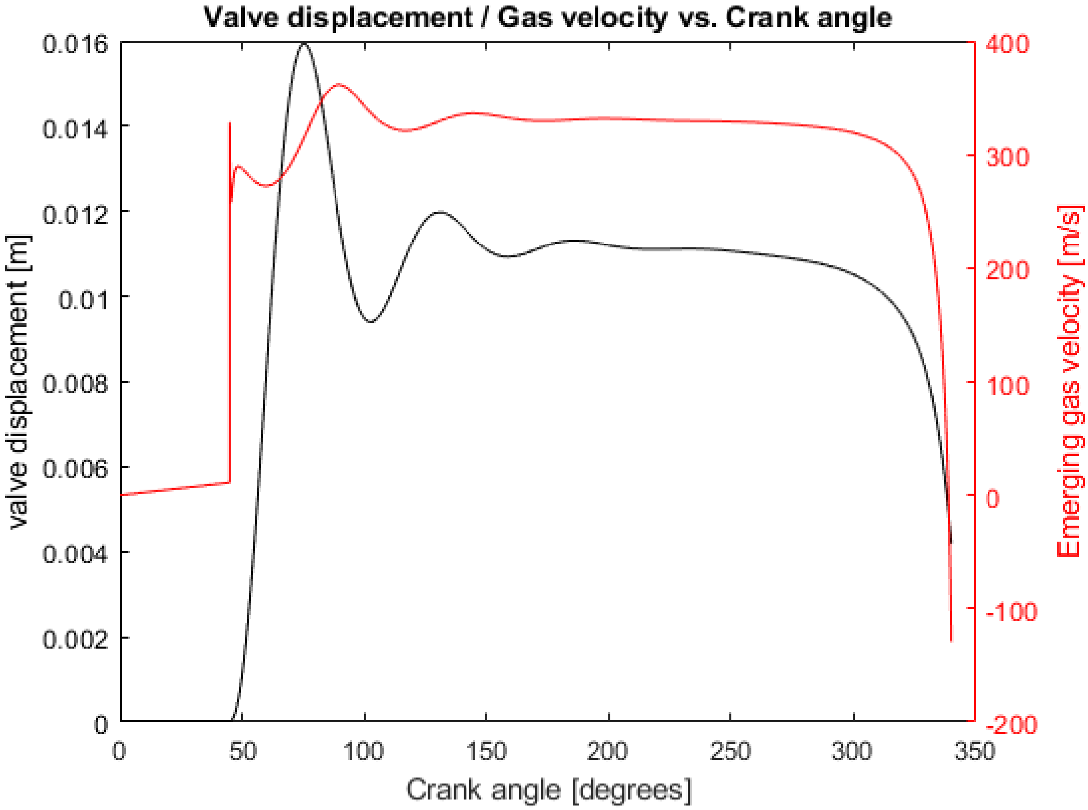

Figure B.3: Illustration of the valve displacement and velocity of emerging gas jet as a function of the crank angle